Advancing functional genetics through *Agrobacterium*-mediated insertional mutagenesis and CRISPR/Cas9 in the commensal and pathogenic yeast *Malassezia furfur*

Giuseppe Ianiri, Gabriel Dagotto, Joseph Heitman*

Department of Molecular Genetics and Microbiology, Duke University Medical Center, Durham, NC, 27710, USA

Running title

Advancing gene studies in *Malassezia*

Key words

Malassezia furfur; insertional mutagenesis; CRISPR/Cas9; protein phosphatase 2A; pleiotropic drug resistance

*Address correspondence to Joseph Heitman, Department of Molecular Genetics and Microbiology, Duke University Medical Center, Durham, North Carolina, United States of America. Phone +1 (919) 684-2824. Fax (919) 684-2790. Email heitm001@duke.edu.

Abstract

Malassezia encompasses a monophyletic group of basidiomycetous yeasts naturally found on the skin of humans and other animals. *Malassezia* species have lost genes for lipid biosynthesis, and are therefore lipid-dependent and difficult to manipulate under laboratory conditions. In this study we applied a recently-developed *Agrobacterium tumefaciens*-mediated transformation protocol to perform T-DNA random insertional mutagenesis in *Malassezia furfur*. A total of 767 transformants were screened after exposure to 10 different stresses, and the 19 mutants that exhibited a phenotype different from the wild type were further characterized. The majority of these strains had single T-DNA insertions, which were identified within the open reading frames of genes, within untranslated regions, and in intergenic regions. Some T-DNA insertions generated chromosomal rearrangements, and others could not be characterized. To validate the findings of the forward genetic screen, a novel CRISPR/Cas9 system was developed to generate targeted deletion mutants for 2 genes identified in the screen: *CDC55* and *PDR10*. This system is based on co-transformation of *M. furfur* mediated by *A. tumefaciens* to deliver both a *CAS9*-gRNA construct that induces double-strand DNA breaks, and a gene replacement allele that serves as a homology directed repair template. Targeted deletion mutants for both *CDC55* and *PDR10* were readily generated with this method. This study demonstrates the feasibility and reliability of *A. tumefaciens*-mediated transformation to aid in the identification of gene functions in *M. furfur* through both insertional mutagenesis and CRISPR/Cas9-mediated targeted gene deletion.

Introduction

The genus *Malassezia* is a lipophilic, monophyletic group of basidiomycetous yeasts that colonize sebaceous skin sites and represents more than 90% of the skin mycobiome (FINDLEY *et al.* 2013; WU *et al.* 2015; BYRD *et al.* 2018). In addition to a ubiquitous presence on the skin of human and animals, recent data support the hypothesis that *Malassezia* fungi are much more widespread than previously thought. Metagenomics studies revealed the presence of *Malassezia* DNA in a number of unexpected areas such as in association with corals and sea sponges in the ocean, although *Malassezia* marine species have yet to be isolated in axenic culture (AMEND *et al.* 2019). There are currently 18 species within the *Malassezia* genus. One defining characteristic of the *Malassezia* genus is the lack of a fatty acid synthase, Δ^9 desaturase, and $\Delta^{2,3}$ enoyl CoA isomerase, making them lipid-dependent and difficult to study and manipulate under laboratory conditions. *Malassezia* are highly divergent from other fungi that are commonly found on the skin, such as *Candida* species and the dermatophytes. Furthermore, *Malassezia* species belong to the Ustilaginomycotina subphylum, which includes the plant pathogens *Ustilago*, *Sporisorium*, and *Tilletia*, and are highly divergent from other basidiomycetous fungi that infect humans, such as *Cryptococcus neoformans*. Recent classifications revealed that *Malassezia* represents a sister group to the blast yeast-like fungi *Moniliella* (WANG *et al.* 2014; WANG *et al.* 2015), which includes species reported to be pathogenic on human and animal skin (MCKENZIE *et al.* 1984; PAWAR *et al.* 2002) as well as others that are of interest in sugar alcohol production in industrial settings (KOBAYASHI *et al.* 2015).

In the last decade, there has been increasing scientific interest in *Malassezia*, with several sequencing projects aimed at defining genomic features and gene content for 15 broadly recognized *Malassezia* species (XU *et al.* 2007; GIOTI *et al.* 2013; TRIANA *et al.* 2015; WU *et al.* 2015; PARK *et al.* 2017; ZHU *et al.* 2017; KIM *et al.* 2018; LORCH *et al.* 2018; CHO *et al.* 2019; MORAND *et al.* 2019). All haploid *Malassezia* species have small genomes compared to other phylogenetically related fungi (7 to 9 Mb compared to ~20 Mb), and have lost genes involved in carbohydrate metabolic processes and hydrolysis activity. Genome analyses have revealed intriguing features, such as i) loss of the RNA interference pathway components; ii) evidence of horizontal gene transfer events from bacteria; iii) the presence of genes unique to *Malassezia*; and iv) the expansion of secreted protein, lipase, and protease gene families that encode products predicted to breakdown lipids and proteins important for growth and host and microbial interactions.

The typical *Malassezia* genome is between ~7 and 9 Mb, which is about half the size of other basidiomycetous fungi, with the exception of *M. furfur* hybrid species whose genomes are twice the size of other *Malassezia* species. It is likely that the genomes of *Malassezia* species have reduced over time concomitantly with their evolution as a commensal organism and adaptation to the skin (WU *et al.* 2015). There are other cases in which fungal genome reduction correlates with niche specialization, with the most remarkable examples being the obligate *Pneumocystis* species with genomes of ~7-8 Mb (MA *et al.* 2016), and *Microsporidia* species with genomes as small as 2.9 Mb (CUOMO *et al.* 2012).

Aside from their commensal lifestyle, *Malassezia* fungi have been associated with several skin disorders, including pityriasis versicolor, dandruff, severe atopic dermatitis

in humans, and otitis in dogs (GAITANIS *et al.* 2012; WU *et al.* 2015). However, the exact role of *Malassezia* in these clinical conditions has been controversial, with recent studies even hypothesizing a protective role of *M. globosa* against *Staphylococcus aureus*, a bacterium that is associated with severe atopic dermatitis (LI *et al.* 2017; IANIRI *et al.* 2018). The lack of knowledge regarding *Malassezia* function within the skin mycobiome is due, in part, to the dearth of experimental systems for studying *Malassezia*-host interactions; current knowledge is based solely on in vitro experiments with isolated host cells (WATANABE *et al.* 2001; ISHIBASHI *et al.* 2006; DONNARUMMA *et al.* 2014; GLATZ *et al.* 2015; SPARBER AND LEIBUNDGUT-LANDMANN 2017). Recently, 2 groundbreaking studies reported novel experimental murine models for studying *Malassezia* interactions with the skin and intestinal mucosa (LIMON *et al.* 2019; SPARBER *et al.* 2019). Sparber and colleagues demonstrated that the application of *M. sympodialis*, *M. pachydermatis*, and *M. furfur* on the dorsal ear skin of mice resulted in robust colonization of the epidermis and a rapid cytokine response dominated by IL-17 and related factors. This response was found to be critical for preventing fungal overgrowth on *Malassezia*-exposed skin and exacerbates inflammation under atopy-like conditions (SPARBER *et al.* 2019). Another study by Limon and colleagues demonstrated the involvement of *Malassezia* in inflammatory bowel disease. The authors characterized the mycobiome associated with the intestinal mucosa of healthy individuals and patients with Crohn's disease, and found that *M. restricta*, one of the most common inhabitants of human skin, was especially abundant in Crohn's disease patients. Moreover, the presence of *M. restricta* was linked with a polymorphism in the gene for CARD9, a signaling adaptor

152 critical for defense against fungi (LIMON *et al.* 2019). The importance of these studies has
153 been highlighted in 2 commentaries (DAWSON 2019; WRIGHTON 2019).

154 Although these models represent an important advance in understanding the
155 mechanisms of host responses to *Malassezia*, a lack of technologies for functional genetic
156 studies has hampered the identification and characterization of the fungal components
157 that promote inflammation and induce host responses. We were the first group to develop
158 a transformation system based on transconjugation-mediated by *Agrobacterium*
159 *tumefaciens* (AtMT, *A. tumefaciens*-mediated transformation) that is effective for both
160 insertional and targeted mutagenesis and enabled the first genetic manipulation of *M.*
161 *furfur* and *M. sympodialis* (IANIRI *et al.* 2016; IANIRI *et al.* 2017). Subsequently, *M.*
162 *pachydermatis* has also been transformed (CELIS *et al.* 2017).

163 CRISPR (clustered regularly interspaced short palindromic repeats)/Cas9 was
164 originally discovered as a mechanism of adaptive bacterial immunity for defense against
165 invading DNA elements (JINEK *et al.* 2012). The CRISPR/Cas9 system has been
166 modified for use in other organisms, and at present, represents a revolutionary technology
167 that has allowed gene editing in a number of cell types, including fungi (SHI *et al.* 2017;
168 ADLI 2018). The system consists of 2 elements: a specific endonuclease (Cas9) and a
169 guide RNA (gRNA) that form a complex that catalyzes double-strand breaks (DSBs) at a
170 specific DNA site flanking a protospacer adjacent motif (PAM) sequence of the host
171 genome. After the DSB is generated, the DNA can be repaired either through non-
172 homologous end joining (NHEJ) or through homology directed repair (HDR) when donor
173 DNA is provided (SHI *et al.* 2017).

The present study is divided into 2 sections. In the first, we build upon the previously developed AtMT technology to perform the first T-DNA-mediated genetic screen in *M. furfur*. The aim was to generate a library of random insertional mutants, select for mutants with a phenotype of interest, and characterize insertion sites within the *M. furfur* genome to infer the function of genes involved in processes of physiological and clinical interest. In the second part of this study, we developed the first efficient, transient CRISPR/Cas9 mutagenesis system for *Malassezia*, and successfully generated targeted deletion mutants of two genes identified in the forward screen: *CDC55*, which encodes a subunit of protein phosphatase 2A (PP2A), and *PDR10*, which encodes an ABC transporter predicted to be involved in pleiotropic drug resistance. When validating the effectiveness of the T-DNA insertional mutagenesis for gene function studies, this novel CRISPR/Cas9 technology overcomes issues related to the reduced rate of homologous recombination observed in *M. furfur*, and we expect that it will facilitate molecular research on *Malassezia* fungi.

Materials and Methods

Strains and culture conditions. The haploid *M. furfur* strain CBS14141 (previously known as JPLK23) was used as the wild type (WT) strain for transformation experiments. This strain was maintained on modified Dixon's media (mDixon) [mycological peptone (10 g/L), malt extract (36 g/L), glycerol (2 ml/L), tween 60 (10 ml/L), desiccated ox-bile (10 g/L) and agar (20g/L) for solid media]. Transformants were maintained on mDixon supplemented with the antifungal agents nourseothricin (NAT) or G418 (NEO).

Forward genetics screen in *M. furfur*. Insertional mutagenesis was performed through AtMT using *Agrobacterium tumefaciens* strain EHA105 engineered with the binary vectors pAIM2 or pAIM6, which contain *NAT* and *NEO* resistance markers under the control of *M. sympodialis ACT1* promoter and terminator, respectively (IANIRI *et al.* 2016). Initially, transformations were performed using previously developed methods (IANIRI *et al.* 2016; CELIS *et al.* 2017). Selected transformants were colony-purified on selective media and arrayed in 96 well plates containing 100 µL of mDixon + NAT or mDixon + NEO for in vitro assays and long-term storage.

For the primary screen, a 1.5 µL aliquot of cellular suspension of transformants was spotted on mDixon agar containing the following chemicals: Congo red (0.5%), sodium chloride (NaCl, 1M), sodium dodecyl sulfate (SDS, 0.3%), or fluconazole (FLC, 150 µg/ml) for cell wall and plasma membrane stress; $NaNO_2$ (100 mM) for nitrosative

stress; or $CdSO_4$ (30 µM) for protein-folding defects and heavy metal stress. Transformants were also exposed to UV light (250 to 450 µJ x 100), elevated temperature (37˚C), pH (pH 7.5), and nutrient-limiting conditions [yeast nitrogen base media (YNB)]; when used, arginine and tyrosine were added at 30 mg/L. Transformants selected in the primary screen as having a phenotype different than the WT were confirmed through a standard 1:10 serial dilution method by spotting 1.5 µL of cellular suspension on mDixon agar in the conditions that allowed their selection.

Molecular characterization of the T-DNA insertional mutants of *M. furfur*. Insertional mutants with a phenotype of interest were single-colony purified and grown overnight in 25 mL of liquid mDixon for genomic DNA extraction using a CTAB extraction buffer (PITKIN *et al.* 1996). To identify the insertion sites of the T-DNA in the *M. furfur* genome, inverse PCR (iPCR) was performed according to previously published methods (IDNURM *et al.* 2004; IANIRI AND IDNURM 2015). Briefly, approximately 2 µg of DNA were digested with the restriction enzymes PvuII, XhoI, SacII, ApaI, EcoRI (6-bp recognition site) or TaqI (4-bp recognition site), column purified, and eluted in 30 µL of elution buffer. Then, 8.5 µL of digested DNA were self-ligated with T4 DNA ligase (New England Biolabs) overnight at 4˚C, and 1 µL was used as template for iPCR using primers ai76-ai77 for DNA digested with restriction enzymes that cut outside the T-DNA region, or ai076-M13F and ai077-M13R where restriction enzymes that cut inside the T-DNA were used (IDNURM *et al.* 2004). iPCR conditions were: initial denaturation at 94˚C for 2 min, denaturation at 94˚C for 30 sec, annealing at 55˚C for 30 sec, and extension at 72˚C for 2.5 min. PCR reactions were performed using ExTaq polymerase (Taqara Bio,

Japan) according to manufacturer's instructions. When ExTaq PCRs were unsuccessful, LaTaq polymerase (Taqara Bio, Japan) suitable for high G+C rich regions was used with an annealing temperature of 55˚C and 60˚C. Amplicons were either PCR- or gel-purified and subjected to Sanger sequencing. Sequences were subjected to BLASTn analysis against the *M. furfur* CBS 14141 genome assembly available on NCBI (reported as JPLK23) (WU *et al.* 2015) and against an unpublished PacBio assembly. Gene boundaries and regulatory regions were determined using unpublished RNAseq data, which allowed us to define the accurate locations of T-DNA insertions. Retrieved *M. furfur* sequences were subjected first to BLASTx analysis against the latest genome assembly of *M. sympodialis* (ZHU *et al.* 2017) and subsequently on SGD (Saccharomyces Genome Database) to identify orthologs and infer gene function. Genes were named based on orthologous genes in *Saccharomyces cerevisiae*. Gene annotation was carried out manually based on BLAST searches and with the automated software Augustus (http://bioinf.uni-greifswald.de/augustus/submission.php) using RNAseq for untranslated regions (UTRs) and introns.

For Southern blot analysis, ~2 µg of genomic DNA were digested with SacII (no cut sites are within the *NAT* or *NEO* cassette, thus allowing us to determine the number of T-DNA insertions), resolved on a 0.8% agarose gel in 1x Tris-acetate EDTA (TAE) buffer, transferred to a Zeta-Probe membrane, and probed with *NAT* or *NEO* cassettes labeled with [^{32}P]dCTP. *NAT* and *NEO* cassettes were amplified from plasmids pAIM2 and pAIM6, respectively, with universal M13F and M13R primers.

RNA extraction was performed using the standard TRIzol method (RIO *et al.* 2010). RNA was treated with the TURBO DNAse enzyme (Thermo Fisher Scientific)

266 according to the manufacturer's instructions, and quality was assessed using a NanoDrop
267 spectrophotometer. Then, 3 µg of purified RNA were converted into cDNA via the
268 Affinity Script QPCR cDNA synthesis kit (Agilent Technologies) according to
269 manufacturer's instructions. For each sample, cDNA synthesized without the RT/RNAse
270 block enzyme mixture was used as a control for genomic DNA contamination.
271 Approximately 500 pg of cDNA were used to measure the relative expression level of
272 target genes through quantitative real-time PCR (RT-qPCR) using the Brilliant III ultra-
273 fast SYBR green QPCR mix (Agilent Technologies) in an Applied Biosystems 7500
274 Real-Time PCR System. For each target, a "no-template control" was performed to
275 analyze melting curves and to exclude primer artifacts. Technical triplicates and
276 biological triplicates were performed for each sample. Gene expression levels were
277 normalized using the endogenous reference gene *TUB2* and determined using the
278 comparative ΔΔCt method.
279
280 **Generation of plasmid for CRIPSR/Cas9 targeted mutagenesis in *M. furfur***
281 Plasmids for targeted mutagenesis of *M. furfur CDC55* and *PDR10* through *A.*
282 *tumefaciens*-mediated transformation were assembled in *S. cerevisiae* using the binary
283 vector pGI3 as previously reported (IANIRI *et al.* 2016; IANIRI *et al.* 2017). The *NAT*
284 cassette was amplified from plasmid pAIM1 using primers JOHE43277 and JOHE43278.
285 The 5′ and 3′ flanking regions for homologous recombination were amplified from the
286 genomic DNA of *M. furfur* CBS14141 using primer pairs JOHE45209-JOHE45210 and
287 JOHE45211-JOHE45212 for *CDC55* and JOHE45201-JOHE45212 and JOHE45203-
288 JOHE45204 for *PDR10*, respectively. The PCR products and the double-digested (KpnI

289 and BamHI) binary vector pGI3 were transformed into S. *cerevisiae* using lithium acetate
290 and PEG 3750 as previously reported (IANIRI *et al.* 2016). To assess correct
291 recombination of the newly generated plasmids, single colonies of *S. cerevisiae*
292 transformants were screened by PCR using primers specific for the *NAT* marker
293 (JOHE43281–JOHE43282) in combination with primers homologous to outside of the
294 region of the plasmid pGI3 involved in the recombination event (JOHE43279-
295 JOHE43280). Positive clones of *S. cerevisiae* were grown ON in YPD and subjected to
296 phenol-chloroform-isoamyl alcohol (25:24:1) plasmid extraction using a previously
297 reported protocol (HOFFMAN 2001). The plasmid DNA obtained was then introduced into
298 the *A. tumefaciens* EHA105 strain by electroporation, and the transformants were
299 selected on LB + 50 µg/mL kanamycin. PCRs were performed using ExTaq and/or
300 LATaq polymerase as described previously, with the only difference being an extension
301 time of 1.5 min.

302 To generate the components of the CRISPR/Cas9 system in *Malassezia*, the
303 histone H3 was identified in the *M. sympodialis* ATCC42132 genome assembly (ZHU *et*
304 *al.* 2017) through BLASTp analysis using *S. cerevisiae* H3 as query. The 813-bp
305 upstream and 257-bp downstream regions, including the *M. sympodialis* H3 promoter and
306 terminator (indicated as p*H3*, and t*H3*), respectively, were amplified by PCR using
307 JOHE46457-JOHE46458, and JOHE46461-JOHE46462, respectively. High Fidelity
308 (HF) Phusion Taq polymerase (New England Biolabs) was used according to
309 manufacturer's instructions, with an annealing temperature of 55°C for 30 sec, and 1 min
310 extension at 72°C. Primer JOHE46457 includes a chimeric region for recombination in
311 pPZP-201BK and a multicloning site, and primers JOHE46458 and JOHE46461 include

312 chimeric regions for recombination with primers JOHE46459 and JOHE46460, which
313 were used to amplify *CAS9* open reading frame (ORF) from plasmid pXL1-Cas9 (FAN
314 AND LIN 2018). Primer JOHE46462 has SacII and SpeI restriction sites, and a region for
315 recombination with the promoter of the 5SrRNA of *M. sympodialis* used to drive
316 expression of the single guide RNA (gRNA). *CAS9* amplification did not work well with
317 HF Phusion Taq, so we used ExTaq polymerase as described above, but with fewer
318 cycles (20 cycles) and a 4-min extension. The *M. sympodialis* ATCC 42132 ribosomal
319 cluster was identified in the latest genome assembly and annotation (ZHU *et al.* 2017)
320 through BLASTn analysis using ITS sequences from *M. sympodialis* CBS 7222 available
321 on GenBank (accession number NR_103583). A 674-bp region from the end of the
322 rRNA-eukaryotic large subunit ribosomal RNA (position 612351 on chromosome 5),
323 including the rRNA-5S ribosomal RNA gene (position 613025 on chromosome 5), was
324 amplified by PCR using primers JOHE46463-JOHE46464. Primer JOHE46463 has a
325 chimeric region complementary to primer JOHE46462. This PCR was performed using
326 the touchdown protocol, with an initial denaturation of 94°C per 5 min, followed by 24
327 cycles of denaturation at 94°C for 30 sec, annealing at a gradient temperature of 62°C for
328 30 sec minus 1°C per cycle, and extension at 72°C for 1 min. This was followed by 16
329 cycles of denaturation at 94°C for 30 sec, annealing at 50°C for 30 sec, extension at 72°C
330 for 1 min, with a final extension of 72°C for 5 min. The gRNA scaffold was amplified
331 from plasmid pSDMA64 (ARRAS *et al.* 2016) using primers JOHE46465-JOHE46466.
332 JOHE46466 includes SpeI and SacII restriction sites, 7 thymine residues (6T terminator),
333 and a chimeric region for recombination in pPZP-201BK.

334 The specific target sequence for *CDC55* was identified using the program
335 EuPaGDT (http://grna.ctegd.uga.edu/) available on FungiDB
336 (https://fungidb.org/fungidb/). Specific target sequence for the gene *CDC55* was added
337 by PCR with primers JOHE46468-JOHE46466 using the gRNA scaffold as template.
338 Primer JOHE46468 has a chimeric region for recombination with both the 5SrRNA
339 sequence and the gRNA scaffold, with an intervening target sequence specific for
340 *CDC55*. These PCRs were performed using HF Phusion Taq as reported above. All
341 components were gel purified, and equimolar amounts of the purified amplicons were
342 used for overlap PCR to generate the Cas9 expression cassette (p*H3*- *CAS9*, t*H3*) and the
343 complete gRNA (5S rRNA promoter fused with the gene-specific gRNA scaffold). PCRs
344 were carried out using HF Phusion taq and the touch down protocol as above, with the
345 only difference being extension times of 5 min and 1 min, respectively. The 2 resulting
346 amplicons were cloned within the T-DNA of pPZP201BK digested with KpnI and
347 BamHI through HiFi (New England Biolabs) assembly according to manufacturer's
348 instructions and recovered in *Escherichia coli* DH5α. *E. coli* clones were screened for
349 recombinant plasmids by PCR using primers specific for the plasmid backbone
350 (JOHE43279 and JOHE43280) in combination with JOHE46458 and JOHE46463,
351 respectively. The plasmid sequence for CRISPR/Cas9 deletion of *CDC55* (named pGI40)
352 was confirmed by Sanger sequencing.

353 To generate the CRISPR/Cas9 plasmid for targeted mutagenesis of *PDR10*, the
354 binary vector pGI40 was digested with SpeI to remove the *CDC55*-specific gRNA,
355 recovered from the gel and purified. A *PDR10*-specific target sequence designed using
356 EuPaGDT was added to the gRNA scaffold by PCR using primers JOHE46466-

JOHE46467, which have chimeric regions for recombination with both the 5SrRNA sequence and the gRNA scaffold, with the specific target sequence for *PDR10* in between.

This amplicon and the 5SrRNA previously generated were recombined through HiFi assembly within the T-DNA of the *Spe*I-digested pGI40, and the novel recombinant plasmids with the *PDR10*-specific gRNA (named pGI48) were identified by Sanger sequencing. This procedure is reported in Figure 4B. Recombinant plasmids were introduced in *A. tumefaciens* through electroporation.

AtMT was performed with modifications that increase transformation efficiency compared to our previous protocol used to generate insertional mutants. Briefly, *M. furfur* was grown for 2 days at 30°C and the culture was diluted to OD_{600} ~1. The engineered *A. tumefaciens* strains with the gene deletion cassettes and the CRISPR/Cas9 expression system were grown overnight, diluted to an OD_{600} ~0.1, and incubated for 4 to 6 h in shaking cultures (30°C) in liquid induction medium (IM) until OD_{600} reached a value of 0.6 to 0.8. These bacterial cellular suspensions were mixed in 1:1, 1:2, and 2:1 ratio, respectively, and they were added to *M. furfur* cellular suspension at 1:2 and 1:5 ratios, respectively. These cellular suspensions were centrifuged at 5200 *g* for 15 min, the supernatants were discarded, and ~500 µl to 1 mL of these fungal and bacterial mixes were spotted directly onto nylon membranes placed on mIM agar containing 200 µM acetosyringone. These were coincubated for 5 days at room temperature (plates maintained without Parafilm) prior to transferring the dual cultures to mDixon supplemented with NAT (100 µg/mL) to select for fungal transformants and cefotaxime (350 µg/mL) to inhibit *Agrobacterium* growth.

M. furfur transformants resistant to NAT were colony purified and subjected to phenotypic and molecular characterization. Putative mutants for the *CDC55* gene were exposed to UV light (250 to 300 µJ x 100) to identify those with impaired growth according to the results of the forward genetic screen. For molecular analysis, 23 representative NAT resistant transformants sensitive to UV light were subjected to phenol-chloroform-isoamyl alcohol (25:24:1) DNA extraction, and the correct replacement of the target loci was assessed by PCR. Diagnostic PCRs to identify homologous recombination events for the *CDC55* gene were carried out with primers JOHE45213 or JOHE45874 in combination with specific primers for the *NAT* gene (JOHE43281 and JOHE43282, respectively), and with primers JOHE45215-JOHE45216 specific for the internal region of *CDC55*. To evaluate the overall rate of homologous recombination (HR) of the CRISPR/Cas9 system, a larger number of *cdc55*Δ candidate mutants were tested for sensitivity to hydroxyurea, which was found to be the stressor with the strongest phenotype. Similarly, putative *pdr10*Δ mutants were exposed to FLC (150 µg/mL) for phenotypic characterization, and transformants displaying impaired growth were subjected to DNA extraction for molecular characterization. Diagnostic PCRs were carried out using primers JOHE45205 and JOHE45206 alone and in combination with specific primers for the *NAT* gene (JOHE43281 and JOHE43282, respectively), and with primers JOHE45207-JOHE45208 specific for the internal region of *PDR10*. PCR analyses consisted of 34 cycles of denaturation at 94˚C for 30 sec, annealing at 55˚C for 30 sec, extension at 72˚C of 1 min/kb, with an initial denaturation at 94˚C for 2 min and a final extension at 72˚C for 5 min. PCR analyses were performed using ExTaq (Takara) according the manufacturer's instructions. To detect homologous

403 recombination events at the 3′ region of *CDC55* and to amplify the full length *PDR10*
404 gene, LATaq polymerase (Takara) with Buffer I was used. PCR for *CAS9* was carried out
405 with ExTaq and the touchdown protocol with primers JOHE46459-JOHE46461. PCR for
406 the gRNA was carried out with JOHE46465-JOHE46466 using ExTaq as reported above.
407 All the primers used are listed in Table S1.

408 Phenotypic analysis of the target mutants was performed on mDixon agar by
409 spotting 1.5 µL of 1:10 dilutions of each cellular suspension in the following conditions:
410 UV (250 to 450 µJ x 100), hydroxyurea (50 mM), benomyl (50 µM), FLC (150 µg/mL),
411 amphotericin B (AmB, 50 µg/mL), 5-flucytosine (5FC, 1 mg/mL), caspofungin (Caspo,
412 100 µg/mL), cyclosporin A (CsA) at 100 µg/mL both alone and in combination with 10
413 mM of lithium chloride, tacrolimus (FK506) at 100 µg/mL both alone and in combination
414 with 10 mM of lithium chloride, and dimethyl sulfoxide (DMSO, 40 µL) which was used
415 to dissolve benomyl (10 mM).

416

417 **Genomic comparison and phylogeny of the ABC transporter of *M. furfur* and *M.***
418 ***sympodialis***

419 The predicted amino acid sequences of *S. cerevisiae* Pdr10, Pdr5, Pdr15, Pdr12,
420 Snq2, Pdr18, Aus1, and Pdr11 were used as queries for tBLASTn and BLASTp searches
421 against the genomes of *M. furfur* CBS14141 and *M. sympodialis* ATCC 42132 available
422 on GenBank (WU *et al.* 2015; ZHU *et al.* 2017). The *Malassezia* best hits were retrieved,
423 and the encoded proteins for *M. furfur* were predicted using Augustus (http://bioinf.uni-
424 greifswald.de/augustus/submission.php) based on RNAseq evidence for UTR regions and
425 introns.

The web portal of ACT Artemis (https://www.webact.org/WebACT/home) was used for synteny analysis of a ~15000 bp region of *M. sympodialis* and *M. furfur* containing orthologues of the Pdr10 encoding genes. tBLASTx analysis with a E-value of 0.100000 was performed.

For phylogeny, the aforementioned predicted ABC transporter proteins were aligned using MUSCLE and the phylogenetic tree was generated with MEGA 7 (http://www.megasoftware.net/) (KUMAR *et al.* 2016) using the maximum likelihood method (LG model, 5 discrete gamma categories) and 100 bootstrap replications.

Results

Molecular and phenotypic characterization of *M. furfur* insertional mutants

Insertional mutants of *M. furfur* were generated through AtMT using both *NAT* and *NEO* dominant drug resistance markers. A total of 767 insertional mutants were isolated and their growth was tested under several different stress conditions. A total of 19 mutants (~2.5%) with a phenotype different than the WT were selected for further characterization.

Inverse PCR (iPCR) was utilized to identify the genes inactivated by the T-DNA insertions. The sequenced amplicons were compared to the unannotated *M. furfur* CBS14141 genome assemblies (one reported in NCBI as *M. furfur* JPLK23, and another unpublished based on PacBio sequencing) coupled with RNAseq data, which facilitated the identification of the coding and regulatory sequences. This allowed an accurate determination of T-DNA insertion sites. Gene names were assigned according to the *Saccharomyces* Genome Database. Southern blot analysis was performed to determine

449 the number of T-DNA insertions, revealing that 16 transformants harbored single T-DNA
450 insertions, and 3 transformants had 2 T-DNA insertions (strains 4A10, 4B1, and 6B2)
451 (Fig. 1). In parallel, iPCR allowed the characterization of 15 T-DNA insertions (Fig. 2).
452 Six strains had T-DNA insertions within a predicted open reading frame (ORF), 2 strains
453 had insertions within UTRs, and 3 strains had T-DNA insertions in intergenic regions
454 with no RNAseq read coverage. Of the remaining 8 strains, 4 were suspected to have
455 chromosomal rearrangements because the T-DNA borders were found in different
456 locations in the *M. furfur* CBS 14141 genome, and the junctions between the T-DNA and
457 the *M. furfur* genome could not be identified in another 4 strains. Table 1 summarizes the
458 results of the forward genetics approach performed in this study, and properties of the T-
459 DNA insertions are reported in Figure 2.

460 Two mutants that displayed reduced growth on YNB were identified, and analysis
461 of the genome sequence flanking the T-DNA revealed insertions in genes involved in
462 amino acid biosynthesis (Fig. 3A). Strain 6C8 had a non-standard T-DNA insertion that
463 generated a deletion of ~800 bp in the genome of *M. furfur*. Moreover, we were not able
464 to identify the sequence of the left border (LB) from iPCR, and the first nucleotides
465 obtained mapped within the ORF of *TYR1*, which encodes prephenate dehydrogenase, an
466 enzyme involved in tyrosine biosynthesis (MANNHAUPT *et al.* 1989). Conversely, the
467 right border (RB) was found within the ORF of the adjacent gene encoding an
468 uncharacterized protein with no conserved domains that shares similarity with several
469 other *Malassezia* species and basidiomycetes. Addition of tyrosine did not restore the
470 growth of strain 6C8 to the WT level (Fig. 3A), which instead was achieved in SD media
471 supplemented with all amino acids, suggesting the hypothesis that Tyr1 is also involved

in the biosynthesis of other amino acids. In strain 2A8, the T-DNA inserted within the ORF of *ARG1*, which encodes the enzyme arginosuccinate synthetase that catalyzes the formation of L-argininosuccinate from citrulline and L-aspartate in the arginine biosynthesis pathway (JAUNIAUX *et al.* 1978). Addition of L-arginine to YNB was sufficient to restore a WT phenotype, confirming that *M. furfur ARG1* is involved in arginine biosynthesis (Fig. 3 A).

Four insertional mutants that showed decreased growth at elevated temperature (37°C) were identified. Of these, only strain 7H6 had a standard T-DNA insertion. In strain 7H6, the T-DNA integrated between 2 genes: downstream of an RNA-binding domain-containing protein and upstream of *JEN1* (Fig 3B). While the RNA-binding domain-containing protein is uncharacterized in *S. cerevisiae*, Jen1 is a plasma membrane monocarboxylate/proton symporter that transports pyruvate, acetate, lactate, and other substrates (CASAL *et al.* 1999). To assess which gene was affected by the T-DNA insertion and therefore responsible for the phenotype of interest, an RT-qPCR analysis was performed. Expression levels were normalized to the *TUB2* gene of *M. furfur* WT grown at 30°C. Expression of the uncharacterized gene encoding the RNA-binding domain-containing protein in strain 7H6 was ~60% lower compared to the WT, whereas expression of *JEN1* was undetectable, indicating that either or both genes could be responsible for the temperature sensitive phenotype of strain 7H6 (Fig 3 B). The other transformants that displayed a temperature-sensitive phenotype included strain 5F1 (which showed a chromosomal rearrangement involving the 5′ regions of the gene *INO80* located on chromosome 1 and of the *GDP1* gene located on chromosome 3), strain 6B2 (which had 2 T-DNA insertions, one of which could be identified and was found within

the ORF of a uncharacterized RhoGTPase), and strain 7D5 (whose T-DNA insertion could not be characterized by iPCR) (Table 1).

Strain 1 A7 showed increased sensitivity to UV light (250 and 350 µJ x 100) compared to WT *M. furfur* CBS 14141 (Fig. 3C). In strain 1A7, the T-DNA inserted into the third exon of the *CDC55* gene. In *S. cerevisiae, CDC55* encodes a regulatory subunit of protein phosphatase 2A. *CDC55* is involved in cell cycle control, and it is required for successful chromosome segregation and nuclear division (HEALY *et al.* 1991; BIZZARI AND MARSTON 2011).

Six strains showed increased sensitivity to the antifungal fluconazole (FLC, 150 µg/ml) compared to the WT strain (Fig. 3D). Strain 6A10 had a T-DNA insertion in the predicted stop codon of the *S. cerevisiae* ortholog *SIP5*. The function of this protein is unknown, and it has no known domains. However, it has been reported to interact with both the Reg1/Glc7 phosphatase and the Snf1 kinase in response to glucose starvation (SANZ *et al.* 2000). In strain 7D9, the T-DNA was found in the intergenic region between the 5′ end of an ATP-binding cassette (ABC) multidrug transporter gene and the 3′ end of the *UBC6* gene. As shown in Figure 6E, the closest *S. cerevisiae* homolog is the ABC transporter *PDR10*, which is the designation that we adopted. ABC multidrug transporters are involved in pleiotropic drug responses that mediate resistance to xenobiotic compounds including mutagens, fungicides, steroids, and anticancer drugs (SIPOS AND KUCHLER 2006). *UBC6* encodes a ubiquitin-conjugating enzyme involved in ER-associated protein degradation (WALTER *et al.* 2001). As confirmed by targeted mutagenesis (discusses below), the FLC-sensitive phenotype of strain 7D9 is due to T-DNA insertion in the promoter region of *PDR10*.

In strain 7F8 the T-DNA inserted within the 3'UTR of *ADY2* (Fig. 3D). *ADY2* encodes an ammonium and acetate transmembrane transporter involved in nitrogen utilization (RABITSCH *et al.* 2001; PAIVA *et al.* 2004). In strain 2H11 T-DNA integration generated a rearrangement involving the *ERG5* gene and the region close to the 5′ end of the *PDA1* gene. In addition to increased sensitivity to FLC, this strain showed increased sensitivity to sodium chloride compared to WT. Erg5 is a cytochrome P450 enzyme that is a C-22 sterol desaturase involved in ergosterol biosynthesis (LEES *et al.* 1995). Although it is known that FLC targets membrane ergosterol, and *ERG5* deletion in *S. cerevisiae* leads to increased FLC sensitivity (KAPITZKY *et al.* 2010), it cannot be excluded that the FLC and NaCl sensitivity of strain 2H11 is due both to *ERG5* mutation and the intrachromosomal rearrangement itself. In strains 2G9 and 5D11, the T-DNA likely integrated in tandem repeats because iPCR amplicons consisted of both the left and right borders of the T-DNA fused together, and this prevented retrieval of the junctions between the T-DNA and the genome.

Three strains showed sensitivity to cadmium sulfate ($CdSO_4$, 30 µM), and only one (strain 2F4) showed a standard T-DNA insertion in the 5′ regions of both *SEC13* and *PRP43* (Fig. 3E). *SEC13* in *S. cerevisiae* encodes an essential protein that is a structural component of the COPII (coat protein complex II), of the nuclear pore outer ring, and of the Seh-1 associated complex. It is involved in COPII-coated vesicle budding from the ER to the Golgi, nuclear pore distribution, and the ubiquitin-dependent ERAD (ER-associated ubiquitin-dependent protein breakdown) pathway, which is involved in protein degradation by cytoplasmic proteasomes (MENON *et al.* 2005; DOKUDOVSKAYA *et al.* 2011; ČOPIČ *et al.* 2012). *S. cerevisiae PRP43* encodes an RNA helicase protein that is

541 also essential for viability and contributes to the biogenesis of ribosomal RNA, and it is
542 also involved in spliceosomal complex disassembly (ARENAS AND ABELSON 1997;
543 GIAEVER *et al.* 2002). qPCR did not show clear downregulation of either gene (data not
544 shown), and whether either or both genes are responsible for the cadmium sulfate-
545 sensitive growth defect remains to be established. Because the T-DNA inserted in the 5′
546 region of *SEC13* and *PRP43,* whose orthologs are essential in *S. cerevisiae*, we speculate
547 that the functions of both genes are affected or that the phenotype observed is unlinked to
548 the T-DNA insertion. In strain 3A1, a rearrangement involving the *JLP2* and *TCP1* genes
549 was found, and for strain 4B1, Southern blot indicated 2 T-DNA insertions, one of which
550 was identified and found within the 3'UTR of the *MAE1* gene, which encodes a
551 mitochondrial malic enzyme that is important for sugar metabolism and acts as a
552 precursor for many amino acids (BOLES *et al.* 1998). For strain 1F12, iPCR using
553 different restriction enzymes was unsuccessful. We also identified a strain (4A10) that
554 was sensitive to sodium nitrite ($NaNO_2$) and SDS. According to Southern blot analysis,
555 strain 4A10 has 2 T-DNA insertions, one of which could be identified and was found in
556 an uncharacterized enoyl-CoA hydratase gene. Another strain (5F10) was sensitive to
557 NaCl and iPCR revealed the presence of a chromosomal rearrangement involving the 3′
558 region of the *DUG1* gene and the 5′ UTR of the *RPC10* gene.
559
560 **Development of a CRISPR/Cas9 gene deletion system to generate *cdc55*Δ *M. furfur***
561 **mutants**
562 To validate the results of the insertional mutagenesis screen, the insertional
563 mutants 1A7 and 7D9 and their mutated genes were chosen for further analysis as a proof

564 of principle. First, we focused on the UV-sensitive strain 1A7 with a T-DNA insertion in
565 the *CDC55* gene. We were intrigued by this strain because *CDC55* mutation is not known
566 to be responsible for UV sensitivity in other fungi. The aim was to generate an *M. furfur*
567 *cdc55*Δ targeted mutant, determine if the UV phenotype of the original insertional mutant
568 is attributable to *CDC55* mutation, and investigate any further functions of the gene in *M.*
569 *furfur*.

570 For targeted mutagenesis of *CDC55*, molecular biology techniques were
571 performed following our previously published methods (IANIRI *et al.* 2016). Regions of
572 1500 and 1000 bp flanking the 5′ and 3′ ends of the *CDC55* target gene, respectively,
573 were amplified from *M. furfur* genomic DNA and fused with the *NAT* marker within the
574 T-DNA borders of plasmid pGI3. The recombinant plasmid (pGI41) bearing the
575 *cdc55*Δ*::NAT* allele was identified in *S. cerevisiae* by colony PCR and *A. tumefaciens*
576 EHA105 transformed by electroporation. Several rounds of *Agrobacterium*-
577 transconjugation were performed, and NAT-resistant transformants of *M. furfur* were
578 single colony-purified and subjected to diagnostic PCR to confirm *CDC55* targeted
579 mutagenesis. None of the transformants tested (0 out of more than 100) showed full
580 replacement of the gene *CDC55*.

581 Next we developed a CRISPR/Cas9 system for *M. furfur* to increase homologous
582 recombination efficiency. Because the plasmid for targeted gene replacement of *CDC55*
583 was already available, we generated an additional plasmid to make a DNA DBS in
584 *CDC55*, and then used the available *cdc55*Δ*::NAT* allele as HDR template to repair the
585 break. For expression of Cas9, the ORF of the *CAS9* endonuclease was cloned under the
586 control of the strong promoter and terminator of the histone *H3* gene of *M. sympodialis*

ATCC42132. To drive expression of gRNA specific for the target *CDC55* gene, the promoter of the 5S rRNA was chosen. Because the ribosomal cluster is well annotated in the newly released genome of *M. sympodialis* (ZHU *et al.* 2017) and we have evidence that *M. sympodialis* promoters and terminators are functional in *M. furfur* (IANIRI *et al.* 2016), a 689 bp region including the 5S rRNA and its upstream region was amplified from *M. sympodialis* ATCC42132. The forward primer for the p5S rRNA contained restriction sites for SacII and SpeI to facilitate genetic manipulations. The scaffold gDNA also was obtained by PCR, and 6 thymine residues (6-T) were included as terminator. A 20-nt oligonucleotide target of gRNA was designed to match a region of the *CDC55* gene adjacent to a PAM site, and it included the 5′ and 3′ regions that overlapped with the 5S rRNA promoter and the gRNA scaffold, respectively. This target oligonucleotide was added to the gRNA scaffold through PCR as reported in Figure 4B. The 5 PCR fragments (p*H3*; *CAS9*; t*H3*; p5S rRNA; gRNA) were used as template for overlap PCRs, and two final amplicons (p*H3*-*CAS9*-t*H3* and p5SrRNA-gRNA) were cloned in pPZP201BK to generate plasmid pGI40 (Table 2) (Figures 4A and 4B).

AtMT of *M. furfur* CBS14141 was conducted to test the developed CRISPR/Cas9 system to generate targeted gene replacement of the *CDC55* gene. Since our previous reports of AtMT of *Malassezia* (IANIRI *et al.* 2016; IANIRI *et al.* 2017), we have optimized the protocol to achieve a higher transformation efficiency. The main change included the use of a 2:1 to 5:1 *Malassezia*:*A. tumefaciens* mixture that was concentrated through centrifugation before the coincubation step on modified induction media [mIM, (IANIRI *et al.* 2016)]. The detailed procedure is reported in the Materials and Methods. For co-transformation of *M. furfur* using *A. tumefaciens* strains bearing the binary vectors

pGI40 (CRISPR/Cas9 expression system) and pGI41 (HDR *cdc55*Δ*::NAT* template), induced bacterial strains were mixed in ratios of 1:1, 1:2, and 2:1, then added to ratios of 1:2 and 1:5 with *M. furfur* cells (Fig. 5A). The co-cultures were centrifuged to eliminate the supernatants, and the pellet containing the mix of the 3 components was spotted on nylon membranes placed on mIM agar. The plates were incubated at room temperature for 5 days without parafilm. The coincubation cultures were recovered and plated on mDixon containing NAT and CEF. A representative subset of 23 *M. furfur* transformants was single colony-purified and subjected to molecular characterization through PCR. Genotyping was performed using 1) primers designed beyond the regions of DNA used in the generation of the deletion allele in combination with specific *NAT* primers; 2) primers internal to the gene *CDC55*; 3) primers specific for the *CAS9* genes, and primers specific for the gRNA (Figure 5B). Specific amplicons of ~1.6 kb and ~1.4 kb for the 5′ (left) and 3′ (right) T-DNA-genomic DNA junctions, respectively, were obtained for all of the 23-randomly selected transformants. Accordingly, the internal region of *CDC55* was amplified only from the WT strain. No amplicons for *CAS9* or the gRNA were obtained. These results indicate that all transformants tested had full replacement of the *CDC55* gene and absence of *CAS9* and gRNA integration in the genome (Fig. 5C). Furthermore, 64 additional random *cdc55*Δ mutant candidates were tested for sensitivity to hydroxyurea, which we found to be the most effective stressor for the *cdc55*Δ phenotype, and found that 62 displayed impaired growth compared to WT (Fig. S1). Therefore, molecular and phenotypic analyses revealed that out of 87 transformants analyzed, 85 were *cdc55*Δ mutants, resulting in a rate of homologous recombination of 97.7%.

In *S. cerevisiae*, *CDC55* positively regulates mitotic entry at the G2/M phase transition and negatively regulates mitotic exit, and it regulates the mitotic spindle assembly and the morphogenesis checkpoint (WANG AND BURKE 1997; BIZZARI AND MARSTON 2011). Null *cdc55*Δ mutants display abnormally elongated buds; decreased growth rate; and increased sensitivity to gamma rays and hydroxyurea (DNA-damaging agents that interfere with DNA replication), to benomyl and nocodazole (which interfere with microtubule polymerization), and cold-induced stress. Phenotypic characterization of 2 representatives independent *cdc55*Δ *M. furfur* mutants confirmed that they were sensitive to UV light (Fig. 5D), corroborating the phenotype of the insertional mutant 1A7. Moreover, the *M. furfur cdc55*Δ mutant had a slower growth rate compared to the WT strain, and increased sensitivity to hydroxyurea and benomyl (Fig. 5D). Due to the inability of *M. furfur* WT to grow at low temperature, cold sensitivity could not be determined for *M. furfur cdc55*Δ. *M. furfur cdc55*Δ mutants were subjected to microscopy analysis both under normal and stress conditions, and when exposed to hydroxyurea they displayed cells with abnormal morphology and elongated buds, similar to *S. cerevisiae cdc55*Δ mutants (Fig. 5E).

Generation of a *pdr10*Δ *M. furfur* mutant with CRISPR/Cas9

The other insertional mutant of interest was strain 7D9, which has a T-DNA insertion between the *PDR10* and *UBC6* genes and exhibited FLC sensitivity. It was hypothesized that the phenotype of strain 7D9 was due to the T-DNA interfering with the function of *PDR10*, which is well known to mediate antifungal drug response and therefore was chosen for targeted mutagenesis. In *M. furfur*, *PDR10* is a large, 4470-bp

gene. The *pdr10*Δ*::NAT* gene disruption cassette was generated as previously described for *CDC55,* and the vector was named pGI42. For the gRNA, a primer with a specific *PDR10* target between regions that overlap with the 5S rRNA promoter and the gRNA scaffold was added to the gRNA scaffold by PCR. The resulting amplicon was then cloned together with the p5S rRNA in the T-DNA of pGI40 digested with SpeI as reported in Figure 4B; this vector was named pGI48.

Co-transformation of *M. furfur* CBS14141 was performed using *A. tumefaciens* strains bearing plasmids pGI42 and pGI48 as reported in Figure 5A. 60 *M. furfur* NAT-R transformants were single colony purified, and streaked onto mDixon + FLC. Five (8.3%) transformants that displayed FLC sensitivity plus a randomly-selected FLC-resistant control strain were subjected to molecular characterization (Fig. 6B). PCR analysis using external screening primers designed beyond the region of DNA utilized to generate the *pdr10*Δ*::NAT* deletion allele produced 2 amplicons: a 6183-bp amplicon for the WT and the FLC resistant strain, and a 3933-bp amplicon for the 5 transformants that displayed FLC sensitivity. For these 5 transformants, PCR carried out using the external primers with specific *NAT* primers generated amplicons of ~1.1 kb and ~1.3 kb on the 5′ and 3′ regions, respectively. PCR using primers internal to the *PDR10* gene generated an amplicon of 486 bp only in the WT and the randomly selected NAT-R strain. These PCR results indicate full replacement of the *PDR10* gene in the 5 transformants that displayed FLC sensitivity.

Mutants *pdr10*Δ showed hypersensitivity to FLC, indicating that the phenotype of strain 7D9 was due to the T-DNA interfering with the function of *PDR10.* Moreover, because ABC transporters are known to be involved in pleiotropic drug resistance and

679 cellular detoxification, the phenotypic response of *pdr10*Δ mutants was tested against
680 other antifungal drugs of clinical relevance. Surprisingly, *M. furfur pdr10*Δ mutants
681 showed only sensitivity to FLC and grew at the WT level on amphotericin B, 5-
682 flucytosine, caspofungin, tacrolimus (FK506), and cyclosporine A (CsA) both alone and
683 in combination with the plasma membrane stressor lithium chloride (Fig. 6C and data not
684 shown), which we previously showed enhances antifungal activity of tacrolimus against
685 *M. furfur* (IANIRI *et al.* 2017). Moreover, *M. furfur pdr10*Δ mutants did not display
686 sensitivity to the DNA-damaging agents UV or hydroxyurea and only displayed
687 sensitivity to the fungicide benomyl (Fig. 6C).

688 During BLAST searches, we noted that *M. furfur* has 2 adjacent ABC transporter-
689 encoding genes that are orthologs of 3 adjacent ABC transporter-encoding genes in *M.*
690 *sympodialis* (Fig. 6D), a *Malassezia* species that we use as a model for genomics
691 comparison within the genus because of the high quality of its genome assembly (ZHU *et*
692 *al.* 2017). Interestingly, BLASTp of these ABC transporters against *S. cerevisiae*
693 revealed high similarity (ie E-value 0.0) with several ABC transporters, such as Pdr18,
694 Pdr12, Pdr5, Pdr10, Pdr15, Aus1, and Pdr11. Reciprocal BLAST (BLASTp and
695 tBLASTn) of these proteins against *M. furfur* and *M. sympodialis* finds only the
696 aforementioned adjacent ABC transporters, which we named *Mf* (*M. furfur*) and *Ms* (*M.*
697 *sympodialis*) *PDR10*_1, *PDR10*_2, and *PDR10*_3. The mutated gene in *M. furfur*
698 corresponds to *PDR10_1*. Phylogenetic analysis revealed that ABC transporters of *M.*
699 *furfur* and *M. sympodialis* cluster together in a maximum likelihood tree and are related
700 to the *S. cerevisiae* Pdr10 ABC transporter, which is the gene designation that we
701 selected. This analysis suggests a common duplication event of the *Malassezia PDR10*

(green dot on Fig. 6E), followed by another more recent duplication in *M. sympodialis* (blue dot on Fig. 6E).

Discussion

A. tumefaciens-mediated transformation is considered a "silver bullet" in functional genomics of fungi, and its main applications as well as the major discoveries that it has allowed have been recently reviewed (IDNURM *et al.* 2017a). Because *A. tumefaciens* can grow under a variety of conditions, the transformation method is versatile and has been successfully applied in a number of fungi, including those with particular nutrient requirements and that are recalcitrant to other transformation approaches, such as *Malassezia* (IANIRI *et al.* 2016; CELIS *et al.* 2017).

In this report, we present the first application of forward genetics in *M. furfur*, a representative species of the fungemia-causing *Malassezia* group. The goal was to generate random insertional mutants, expose them to stress conditions to isolate those displaying sensitivity compared to the WT, and identify the corresponding T-DNA insertion sites to determine the function of the genes causing the phenotypes. Given the lack of knowledge on gene function in *Malassezia*, insertional mutants were assayed on a variety of conditions that are known to interfere with i) important cellular processes, such as those involved in plasma membrane and cell wall maintenance, growth under nutrient limiting conditions, and protein folding; ii) response to environmental stresses, such as osmotic and nitrosative stresses, UV light, elevated temperature and pH, and heavy metals; and iii) response to the antifungal FLC, which is of clinical relevance.

This loss-of-function screen allowed the characterization of 8 *M. furfur* insertional mutants (1A7, 2A8, 2F4, 6A10, 6C8, 7D9, 7F8, 7H6) that had 1 T-DNA insertion as determined by Southern blot analysis (Fig. 1) and that displayed sensitivity to one or more stress conditions (Fig. 3; Table 1). In 4 strains, the T-DNA inserted within the ORF of genes, and in another it was found to lie within a 3′ UTR (Table 1, Fig. 2 - 3), thus allowing us to define with high probability a direct link between genotype and phenotype. Clear examples of this were *M. furfur* transformants 2A8 and 1A7. Strain 2A8 was selected because of its reduced growth on minimal medium (YNB), and it was found to have a T-DNA insertion in the *ARG1* gene. Strain 1A7 was selected for its increased sensitivity to UV light, and found to have a T-DNA insertion in the *CDC55* gene. Two different approaches were employed to validate the findings of the insertional mutagenesis screen. For strain 2A8 the addition of arginine was sufficient to rescue

747 growth to a WT level (Fig. 3A), while for strain 1A7, targeted *M. furfur cdc55*Δ mutants
748 (Fig. 5) confirmed UV sensitivity.

749 In 3 other mutants of interest, the T-DNA inserted between 2 adjacent genes, and
750 further experiments were conducted to identify the gene(s) responsible for the observed
751 phenotype. A successful approach for strain 7H6 was gene expression analysis through
752 RT-qPCR, which revealed downregulation of both genes flanking the T-DNA insertion
753 (Fig. 3B). Strain 7D9 was sensitive to FLC and had a T-DNA insertion between the 3′
754 region of *UBC6* and 5′ region of *PDR10*, and targeted mutagenesis confirmed that the
755 observed phenotype was due to T-DNA insertion in the promoter region of *PDR10* (Fig.
756 6). Lastly, the RT-qPCR approach did not allow us to define which genes was responsible
757 for the cadmium sulfate sensitive phenotype of strain 2F4 (data not shown).

758 Despite the benefits of an AtMT random mutagenesis approach, analysis of the T-
759 DNA insertion events also revealed limitations. Eleven of 19 *M. furfur* insertional
760 mutants selected (~58%) were not useful for gene function analysis. Three transformants
761 had 2 T-DNA insertions as determined by Southern blot analysis (Fig. 1), and although
762 we determined at least one insertion site (Table 1), it was not possible to determine which
763 gene was responsible for the mutant phenotype. Moreover, the insertion sites could not be
764 identified through iPCR for 2 transformants (1F12 and 7D5). Strains 2G9 and 5D11
765 contained tandem T-DNA insertions, and in 4 strains (2H11, 3A1, 5F1, 5F10),
766 chromosomal rearrangements following the integration of the T-DNA in the *M. furfur*
767 genome were observed. Although AtMT represents a powerful method for random
768 mutagenesis, we and other authors have commonly found non-standard T-DNA insertion
769 events in the genome of both ascomycetous and basidiomycetous fungi [for more details

770 see the following reviews and references within them (MICHIELSE *et al.* 2005; BOURRAS
771 *et al.* 2015; IDNURM *et al.* 2017a; HOOYKAAS *et al.* 2018)]. For example, in a recent study
772 on systematic T-DNA insertion events in the red yeast *Rhodosporidium toruloides*,
773 Coradetti and colleagues found that only 13% of mutants had regular T-DNA insertions
774 and a total of 21% of insertions were useful to identify the genes mutated by the T-DNA
775 (CORADETTI *et al.* 2018). Moreover, in classical forward genetic screens in which loss-of-
776 function events are selected, it is common to isolate strains with chromosomal
777 rearrangements that originated following the insertion of the T-DNA, because these
778 strains are generally less fit and display increased sensitivity to stress (IANIRI AND
779 IDNURM 2015). These undesirable events have been also described following AtMT of
780 plants (CLARK AND KRYSAN 2010).

781 Typically in forward genetics the linkage between the T-DNA insertion and the
782 phenotype is confirmed through: 1) sexual crosses and analysis of the phenotype in the
783 recombinant progeny, 2) functional complementation, or 3) generation an independent
784 targeted mutation for the gene identified (IDNURM *et al.* 2017a). Because of the lack of a
785 known sexual cycle in *Malassezia*, and the difficulty of genetic manipulations for
786 complementation studies, in the present study we aimed to generate *M. furfur* mutants for
787 the genes *CDC55* and *PDR10* to validate their involvement in UV and FLC resistance,
788 respectively. Following our previously reported protocol for targeted mutagenesis in *M.*
789 *furfur* (IANIRI *et al.* 2016; IANIRI *et al.* 2017), several transformation rounds were
790 performed, but we did not obtain any *CDC55* or *PDR10* mutants. Therefore, a system
791 based on CRISPR/Cas9 was developed to increase homologous recombination and
792 facilitate the generation of targeted mutants in *M. furfur*.

793 Because AtMT is the only effective transformation technique for *Malassezia*, a
794 functional *CAS9* cassette and a gRNA needed to be cloned within the T-DNA of a binary
795 vector, together with a marker for selection. For homologous recombination-mediated
796 targeted mutagenesis, a specific gene replacement construct to serve as template to repair
797 the BSB was also necessary. Cloning of all the required components within the T-DNA
798 of one binary vector is technically challenging and time consuming. In one study, Kujoth
799 and colleagues generated a large T-DNA that included one or more gRNA, a Cas9
800 expression cassette, and a gene marker, and successfully applied this system in gene
801 editing strategies through NHEJ in *Blastomyces dermatitidis* (KUJOTH *et al.* 2018). For
802 CRISPR/Cas9 in *Leptosphaeria maculans*, Idnurm and colleagues reported a system
803 based on 2 binary vectors, one with *CAS9* and a marker, and the other with gRNA and
804 another marker, that could be successfully delivered at the same time through co-
805 transformation employing *A. tumefaciens* to perform efficient gene editing through NHEJ
806 (IDNURM *et al.* 2017b). For CRISPR/Cas9 of *Malassezia*, we opted for a system that
807 would be suitable for targeted gene replacement through homologous recombination
808 based on co-transformation of *M. furfur* with 2 *A. tumefaciens* strains, one bearing the
809 binary vector with the HDR gene deletion allele, and another with a binary vector
810 engineered for the CRISPR/Cas9 system without a gene marker. The rationale for
811 generating a marker-free binary vector was to: 1) have a CRISPR/Cas9 transient
812 expression system with a reduced rate of *CAS9* and/or gRNA ectopic integration in the
813 host genome, similar to a system developed for *C. albicans* and *C. neoformans* (MIN *et*
814 *al.* 2016; FAN AND LIN 2018); 2) allow further genetic manipulation of the *NAT*-generated
815 mutant using the other *Malassezia*-specific gene marker available, which encodes for

816 resistance to neomycin; and 3) reduce recombination within the actin promoter and
817 terminator regions of the *NAT* and *NEO* gene markers.

818 Considering gRNA expression, the choice of an appropriate promoter has
819 represented a major challenge for the application of CRISPR/Cas9 technology in fungi.
820 Currently, common approaches include the use of a strong promoter recognized by RNA
821 polymerase II, such as that of the *ACT1* or *GDP1* genes, coupled with a hammerhead
822 ribozyme and/or hepatitis delta virus ribozyme for gRNA excision (IDNURM *et al.* 2017b;
823 KUJOTH *et al.* 2018); the use of RNA polymerase III promoters, such as the U6 promoters
824 of small nuclear RNA used for *C. neoformans* (WANG *et al.* 2016; FAN AND LIN 2018);
825 or the promoters of the tRNA or rRNA with or without ribozymes (SHI *et al.* 2017). In
826 this study, we first tested a strategy based on the use of the 5S rRNA promoter of *M.*
827 *sympodialis* (Fig. 4B). While we were working on developing this system, Zheng and
828 colleagues reported a similar approach in *A. niger*, demonstrating high efficiency of gene
829 editing using both the 5S rRNA promoter alone or combined with the HDV ribozyme
830 (ZHENG *et al.* 2018). Cas9 expression is usually achieved using a strong promoter and
831 terminator; in this study the regulatory regions of the histone *H3* gene of *M. sympodialis*
832 served this purpose (Fig. 4A). During the first CRISPR/Cas9 attempt, we were able to
833 generate *M. furfur cdc55*Δ mutants. Surprisingly, both molecular and phenotypic analysis
834 revealed a homologous recombination rate of 98% (Fig 4C, and Fig. S1). This high rate
835 of homologous recombination is similar to that in the study of Zheng and colleagues
836 (ZHENG *et al.* 2018) and other CRISPR/Cas9-mediated gene deletion approaches (FAN
837 AND LIN 2018). Given these positive results, the use of ribozymes flanking the 5S rRNA
838 promoter was not tested. Phenotypic analysis confirmed the involvement of *CDC55* in

UV resistance, and further assays revealed sensitivity of the *M. furfur cdc55*Δ mutant to benomyl and hydroxyurea (Fig. 5D), which also induced an abnormal bud morphology (Fig. 5E). This indicates a conserved function of the cell division cycle protein Cdc55 in *M. furfur* and *S. cerevisiae.*

This CRISPR/Cas9 technology was then tested for targeted mutagenesis of another gene of interest, *PDR10*. Corroborating results obtained for *CDC55*, we were able to promptly obtain *pdr10*Δ mutants, although the rate of homologous recombination was lower for this gene. This could be due to several factors, such as shorter flanking regions of ~800 bp used in the HDR *pdr10*Δ*::NAT* template, the length of the *PDR10* gene (more than 4 Kb), the genomic location, or to lower activity of the *PDR10*-specific gRNA. Analysis of *M. furfur pdr10*Δ mutants revealed an unexpected specificity of *M. furfur PDR10* for resistance to the clinical-relevant drug FLC, and to the antifungal agent benomyl (Fig. 6C). While there are multiple studies on the pleiotropic drug resistance function of ABC transporters in non-pathogenic (*S. cerevisiae*) and pathogenic (*C. albicans*) yeasts (SIPOS AND KUCHLER 2006; COSTE *et al.* 2008; PAUL AND MOYE-ROWLEY 2014), in these cases specific analysis of Pdr10 in response to several drugs has yet to be performed, and therefore it is not possible to provide a detailed comparison analysis that supports conserved or divergent functions of *PDR10* in *M. furfur.* A recent study reported the involvement of *S. cerevisiae* Pdr10 in double-strand break repair via sister chromatid exchange (MUÑOZ-GALVÁN *et al.* 2013), but we could not confirm this function in *M. furfur* because of the lack of sensitivity of *pdr10*Δ mutants to DNA-damaging agents (Fig. 5C). Further bioinformatics analyses revealed that Pdr10 is the only ABC transporter present in the genome of two *Malassezia* species, and that it

underwent ancestral and more recent gene duplication events (Fig. 6D-E). This suggests profound differences with other fungi, and further studies are needed to elucidate the evolution and specific roles of these *Malassezia* ABC transporters in resistance to chemicals and their network of interactions.

Our understanding of *Malassezia* genetics is still limited, and the T-DNA-mediated random insertional mutagenesis applied in this study coupled with a novel and efficient CRISPR/Cas9 system represent straightforward approaches to advance molecular genetics in this understudied organism. Indeed, while T-DNA-mediated random insertional mutagenesis is of particular relevance to discover novel gene functions, such as the UV sensitive phenotype of *CDC55*, or the FLC sensitivity due to mutations in the genes *SIP5* and *ADY2*, the efficiency of CRISPR/Cas9 is a critical requirement to perform large-scale analyses while also validating the results of the genetics screen.

Historically *Malassezia* research has been hampered by the fastidious nature and particular growth requirements of species within this genus and by their difficult identification and classification. Nevertheless, in addition to the available genome sequence and annotation of most *Malassezia* species, the recent introduction of animal models to study *Malassezia* interactions with the skin and the gastrointestinal tract (LIMON *et al.* 2019; SPARBER *et al.* 2019), and the development of this novel CRISPR/Cas9 system and other existing molecular technologies (IANIRI *et al.* 2016; CELIS *et al.* 2017; IANIRI *et al.* 2017) represent key scientific advances to study the biology and pathophysiology of *Malassezia*, the main fungal inhabitants of mammalian skin.

ACKNOWLEDGMENTS

We thank Sheng Sun for assistance with Southern blot analysis, and Tom Dawson for sharing unpublished genome and RNAseq information prior to publication. We thank Ci Fu, Shelby Priest and Cecelia Wall for critical comments on the manuscript.

FUNDING INFORMATION

This work was supported by NIH/NIAID R01 grant AI50113-15 and by NIH/NIAID R37 MERIT award AI39115-21 (to J.H.).

References

Adli, M., 2018 The CRISPR tool kit for genome editing and beyond. Nature Communications 9**:** 1911.

Amend, A., G. Burgaud, M. Cunliffe, V. P. Edgcomb, C. L. Ettinger *et al.*, 2019 Fungi in the marine environment: open questions and unsolved problems. mBio 10**:** e01189-01118.

911 Arenas, J. E., and J. N. Abelson, 1997 Prp43: An RNA helicase-like factor involved in
912 spliceosome disassembly. Proceedings of the National Academy of Sciences
913 94**:** 11798-11802.
914 Arras, S. D., S. M. Chua, M. S. Wizrah, J. A. Faint, A. S. Yap *et al.*, 2016 Targeted genome
915 editing via CRISPR in the pathogen *Cryptococcus neoformans*. PLoS One 11**:**
916 e0164322.
917 Bizzari, F., and A. L. Marston, 2011 Cdc55 coordinates spindle assembly and
918 chromosome disjunction during meiosis. J Cell Biol 193**:** 1213-1228.
919 Boles, E., P. de Jong-Gubbels and J. T. Pronk, 1998 Identification and
920 Characterization of *MAE1*, the *Saccharomyces cerevisiae* structural gene
921 encoding mitochondrial malic enzyme. Journal of Bacteriology 180**:** 2875-
922 2882.
923 Bourras, S., T. Rouxel and M. Meyer, 2015 *Agrobacterium tumefaciens* gene transfer:
924 how a plant pathogen hacks the nuclei of plant and nonplant organisms.
925 Phytopathology 105**:** 1288-1301.
926 Byrd, A. L., Y. Belkaid and J. A. Segre, 2018 The human skin microbiome. Nat Rev
927 Microbiol 16**:** 143-155.
928 Casal, M., S. Paiva, R. P. Andrade, C. Gancedo and C. Leão, 1999 The lactate-proton
929 symport of *Saccharomyces cerevisiae* is encoded by *JEN1*. Journal of
930 Bacteriology 181**:** 2620-2623.
931 Celis, A. M., A. M. Vos, S. Triana, C. A. Medina, N. Escobar *et al.*, 2017 Highly efficient
932 transformation system for *Malassezia furfur* and *Malassezia pachydermatis*
933 using *Agrobacterium tumefaciens*-mediated transformation. J Microbiol
934 Methods 134**:** 1-6.
935 Cho, Y.-J., M. Park and W. H. Jung, 2019 Resequencing the genome of *Malassezia*
936 *restricta s*train KCTC 27527. Microbiology Resource Announcements 8**:**
937 e00213-00219.
938 Clark, K. A., and P. J. Krysan, 2010 Chromosomal translocations are a common
939 phenomenon in *Arabidopsis thaliana* T-DNA insertion lines. Plant J 64**:** 990-
940 1001.
941 Čopič, A., C. F. Latham, M. A. Horlbeck, J. G. D'Arcangelo and E. A. Miller, 2012 ER
942 cargo properties specify a requirement for COPII coat rigidity mediated by
943 Sec13p. Science 335**:** 1359-1362.
944 Coradetti, S. T., D. Pinel, G. M. Geiselman, M. Ito, S. J. Mondo *et al.*, 2018 Functional
945 genomics of lipid metabolism in the oleaginous yeast *Rhodosporidium*
946 *toruloides*. Elife 7: e32110.
947 Coste, A. T., M. Ramsdale, F. Ischer and D. Sanglard, 2008 Divergent functions of
948 three *Candida albicans* zinc-cluster transcription factors (*CTA4, ASG1* and
949 *CTF1*) complementing pleiotropic drug resistance in *Saccharomyces*
950 *cerevisiae*. Microbiology 154**:** 1491-1501.
951 Cuomo, C. A., C. A. Desjardins, M. A. Bakowski, J. Goldberg, A. T. Ma *et al.*, 2012
952 Microsporidian genome analysis reveals evolutionary strategies for obligate
953 intracellular growth. Genome Res 22**:** 2478-2488.
954 Dawson, T. L., 2019 *Malassezia*: The forbidden kingdom opens. Cell Host & Microbe
955 25**:** 345-347.

956 Dokudovskaya, S., F. Waharte, A. Schlessinger, U. Pieper, D. P. Devos *et al.*, 2011 A
957 conserved coatomer-related complex containing Sec13 and Seh1 dynamically
958 associates with the vacuole in *Saccharomyces cerevisiae*. Molecular & Cellular
959 Proteomics 10**:** M110. 006478.
960 Donnarumma, G., B. Perfetto, I. Paoletti, G. Oliviero, C. Clavaud *et al.*, 2014 Analysis
961 of the response of human keratinocytes to *Malassezia globosa* and *restricta*
962 strains. Arch Dermatol Res 306**:** 763-768.
963 Fan, Y., and X. Lin, 2018 Multiple Applications of a transient CRISPR-Cas9 coupled
964 with electroporation (TRACE) system in the *Cryptococcus neoformans* species
965 complex. Genetics 208**:** 1357-1372.
966 Findley, K., J. Oh, J. Yang, S. Conlan, C. Deming *et al.*, 2013 Topographic diversity of
967 fungal and bacterial communities in human skin. Nature 498**:** 367-370.
968 Gaitanis, G., P. Magiatis, M. Hantschke, I. D. Bassukas and A. Velegraki, 2012 The
969 *Malassezia* genus in skin and systemic diseases. Clinical Microbiology
970 Reviews 25**:** 106-141.
971 Giaever, G., A. M. Chu, L. Ni, C. Connelly, L. Riles *et al.*, 2002 Functional profiling of
972 the *Saccharomyces cerevisiae* genome. Nature 418**:** 387.
973 Gioti, A., B. Nystedt, W. Li, J. Xu, A. Andersson *et al.*, 2013 Genomic insights into the
974 atopic eczema-associated skin commensal yeast *Malassezia sympodialis*.
975 mBio 4**:** e00572-00512.
976 Glatz, M., P. P. Bosshard, W. Hoetzenecker and P. Schmid-Grendelmeier, 2015 The
977 Role of *Malassezia* spp. in atopic dermatitis. Journal of Clinical Medicine 4**:**
978 1217-1228.
979 Healy, A. M., S. Zolnierowicz, A. E. Stapleton, M. Goebl, A. A. Depaoli-Roach *et al.*,
980 1991 *CDC55*, a *Saccharomyces cerevisiae* gene involved in cellular
981 morphogenesis: identification, characterization, and homology to the B
982 subunit of mammalian type 2A protein phosphatase. Molecular and Cellular
983 Biology 11**:** 5767-5780.
984 Hoffman, C. S., 2001 Preparation of Yeast DNA in *Current Protocols in Molecular*
985 *Biology*. John Wiley & Sons, Inc.
986 Hooykaas, P. J. J., G. P. H. van Heusden, X. Niu, M. Reza Roushan, J. Soltani *et al.*, 2018
987 Agrobacterium-mediated transformation of yeast and fungi, pp. 349-374 in
988 *Agrobacterium Biology: From Basic Science to Biotechnology*, edited by S. B.
989 Gelvin. Springer International Publishing, Cham.
990 Ianiri, G., S. Applen Clancey, S. C. Lee and J. Heitman, 2017 FKBP12-dependent
991 inhibition of calcineurin mediates immunosuppressive antifungal drug action
992 in *Malassezia*. mBio 8**:** e01752-01717.
993 Ianiri, G., A. F. Averette, J. M. Kingsbury, J. Heitman and A. Idnurm, 2016 Gene
994 function analysis in the ubiquitous human commensal and pathogen
995 *Malassezia* genus. mBio 7**:** e01853-01816.
996 Ianiri, G., J. Heitman and A. Scheynius, 2018 The skin commensal yeast *Malassezia*
997 *globosa* thwarts bacterial biofilms to benefit the host. J Invest Dermatol 138**:**
998 1026-1029.
999 Ianiri, G., and A. Idnurm, 2015 Essential gene discovery in the basidiomycete
1000 *Cryptococcus neoformans* for antifungal drug target prioritization. mBio 6**:**
1001 e02334-02314.

1002 Idnurm, A., A. M. Bailey, T. C. Cairns, C. E. Elliott, G. D. Foster *et al.*, 2017a A silver
1003 bullet in a golden age of functional genomics: the impact of *Agrobacterium*-
1004 mediated transformation of fungi. Fungal Biology and Biotechnology 4**:** 6.
1005 Idnurm, A., J. L. Reedy, J. C. Nussbaum and J. Heitman, 2004 *Cryptococcus neoformans*
1006 virulence gene discovery through insertional mutagenesis. Eukaryotic Cell 3**:**
1007 420-429.
1008 Idnurm, A., A. S. Urquhart, D. R. Vummadi, S. Chang, A. P. Van de Wouw *et al.*, 2017b
1009 Spontaneous and CRISPR/Cas9-induced mutation of the osmosensor
1010 histidine kinase of the canola pathogen *Leptosphaeria maculans*. Fungal
1011 Biology and Biotechnology 4**:** 12.
1012 Ishibashi, Y., T. Sugita and A. Nishikawa, 2006 Cytokine secretion profile of human
1013 keratinocytes exposed to *Malassezia* yeasts. FEMS Immunology & Medical
1014 Microbiology 48**:** 400-409.
1015 Jauniaux, J.-C., L. A. Urrestarazu and J.-M. Wiame, 1978 Arginine metabolism in
1016 *Saccharomyces cerevisiae*: subcellular localization of the enzymes. Journal of
1017 bacteriology 133**:** 1096-1107.
1018 Jinek, M., K. Chylinski, I. Fonfara, M. Hauer, J. A. Doudna *et al.*, 2012 A programmable
1019 dual-RNA–guided DNA endonuclease in adaptive bacterial immunity. Science
1020 337**:** 816-821.
1021 Kapitzky, L., P. Beltrao, T. J. Berens, N. Gassner, C. Zhou *et al.*, 2010 Cross - species
1022 chemogenomic profiling reveals evolutionarily conserved drug mode of
1023 action. Molecular Systems Biology 6**:** 451.
1024 Kim, M., Y. J. Cho, M. Park, Y. Choi, S. Y. Hwang *et al.*, 2018 Genomic tandem
1025 quadruplication is associated with ketoconazole resistance in *Malassezia*
1026 *pachydermatis*. J Microbiol Biotechnol 28**:** 1937-1945.
1027 Kobayashi, Y., H. Iwata, D. Mizushima, J. Ogihara and T. Kasumi, 2015 Erythritol
1028 production by *Moniliella megachiliensis* using nonrefined glycerol waste as
1029 carbon source. Lett Appl Microbiol 60**:** 475-480.
1030 Kujoth, G. C., T. D. Sullivan, R. Merkhofer, T.-J. Lee, H. Wang *et al.*, 2018 CRISPR/Cas9-
1031 mediated gene disruption reveals the importance of zinc metabolism for
1032 fitness of the dimorphic fungal pathogen *Blastomyces dermatitidis*. mBio 9**:**
1033 e00412-00418.
1034 Kumar, S., G. Stecher and K. Tamura, 2016 MEGA7: Molecular evolutionary genetics
1035 analysis version 7.0 for bigger aatasets. Mol Biol Evol 33**:** 1870-1874.
1036 Lees, N., B. Skaggs, D. Kirsch and M. Bard, 1995 Cloning of the late genes in the
1037 ergosterol biosynthetic pathway of *Saccharomyces cerevisiae*—A review.
1038 Lipids 30**:** 221-226.
1039 Li, H., B. Goh, W. K. Teh, Z. Jiang, J. P. Z. Goh *et al.*, 2017 Skin commensal *Malassezia*
1040 *globosa* secreted protease attenuates *Staphylococcus aureus* biofilm
1041 formation. J Invest Dermatol 138:1137-1145.
1042 Limon, J. J., J. Tang, D. Li, A. J. Wolf, K. S. Michelsen *et al.*, 2019 *Malassezia* is
1043 associated with Crohn's disease and exacerbates colitis in mouse models. Cell
1044 Host & Microbe 25**:** 377-388.e376.
1045 Lorch, J. M., J. M. Palmer, K. J. Vanderwolf, K. Z. Schmidt, M. L. Verant *et al.*, 2018
1046 *Malassezia vespertilionis* sp. nov.: a new cold-tolerant species of yeast

1047 isolated from bats. Persoonia - Molecular Phylogeny and Evolution of Fungi
1048 41**:** 56-70.
1049 Ma, L., Z. Chen, W. Huang da, G. Kutty, M. Ishihara *et al.*, 2016 Genome analysis of
1050 three *Pneumocystis* species reveals adaptation mechanisms to life exclusively
1051 in mammalian hosts. Nat Commun 7**:** 10740.
1052 Mannhaupt, G., R. Stucka, U. Pilz, C. Schwarzlose and H. Feldmann, 1989
1053 Characterization of the prephenate dehydrogenase-encoding gene, *TYR1*,
1054 from *Saccharomyces cerevisiae*. Gene 85**:** 303-311.
1055 McKenzie, R. A., M. D. Connole, M. R. McGinnis and R. Lepelaar, 1984 Subcutaneous
1056 phaeohyphomycosis caused by *Moniliella suaveolens* in two cats. Veterinary
1057 Pathology 21**:** 582-586.
1058 Menon, B. B., N. J. Sarma, S. Pasula, S. J. Deminoff, K. A. Willis *et al.*, 2005 Reverse
1059 recruitment: the Nup84 nuclear pore subcomplex mediates Rap1/Gcr1/Gcr2
1060 transcriptional activation. Proceedings of the National Academy of Sciences
1061 102**:** 5749-5754.
1062 Michielse, C. B., P. J. Hooykaas, C. A. v. a. n. d. e. n. Hondel and A. F. Ram, 2005
1063 *Agrobacterium*-mediated transformation as a tool for functional genomics in
1064 fungi. Curr Genet 48:1-17.
1065 Min, K., Y. Ichikawa, C. A. Woolford and A. P. Mitchell, 2016 *Candida albicans* gene
1066 deletion with a transient CRISPR-Cas9 system. mSphere 1**:** e00130-00116.
1067 Morand, S. C., M. Bertignac, A. Iltis, I. C. R. M. Kolder, W. Pirovano *et al.*, 2019
1068 Complete genome sequence of *Malassezia restricta* CBS7877, an opportunist
1069 pathogen involved in dandruff and seborrheic dermatitis. Microbiology
1070 Resource Announcements 8**:** e01543-01518.
1071 Muñoz-Galván, S., S. Jimeno, R. Rothstein and A. Aguilera, 2013 Histone H3K56
1072 acetylation, Rad52, and non-DNA repair factors control double-strand break
1073 repair choice with the sister chromatid. PLoS Genetics 9**:** e1003237.
1074 Paiva, S., F. Devaux, S. Barbosa, C. Jacq and M. Casal, 2004 Ady2p is essential for the
1075 acetate permease activity in the yeast *Saccharomyces cerevisiae*. Yeast 21**:**
1076 201-210.
1077 Park, M., Y. J. Cho, Y. W. Lee and W. H. Jung, 2017 Whole genome sequencing analysis
1078 of the cutaneous pathogenic yeast *Malassezia restricta* and identification of
1079 the major lipase expressed on the scalp of patients with dandruff. Mycoses
1080 60**:** 188-197.
1081 Paul, S., and W. S. Moye-Rowley, 2014 Multidrug resistance in fungi: regulation of
1082 transporter-encoding gene expression. Frontiers in Physiology 5: 143.
1083 Pawar, S., D. Murray, W. Khalife, B. Robinson-Dunn and M. McGinnis, 2002 Human
1084 infection caused by *Moniliella suaveolens*. Clinical Microbiology Newsletter
1085 24**:** 53-55.
1086 Pitkin, J. W., D. G. Panaccione and J. D. Walton, 1996 A putative cyclic peptide efflux
1087 pump encoded by the *TOXA* gene of the plant-pathogenic fungus *Cochliobolus*
1088 *carbonum.* Microbiology 142**:** 1557-1565.
1089 Rabitsch, K. P., A. Tóth, M. Gálová, A. Schleiffer, G. Schaffner *et al.*, 2001 A screen for
1090 genes required for meiosis and spore formation based on whole-genome
1091 expression. Current Biology 11**:** 1001-1009.

Rio, D. C., M. Ares, G. J. Hannon and T. W. Nilsen, 2010 Purification of RNA using TRIzol (TRI reagent). Cold Spring Harbor Protocols 2010**:** pdb. prot5439.

Sanz, P., K. Ludin and M. Carlson, 2000 Sip5 interacts with both the Reg1/Glc7 protein phosphatase and the Snf1 protein kinase of *Saccharomyces cerevisiae*. Genetics 154**:** 99-107.

Shi, T.-Q., G.-N. Liu, R.-Y. Ji, K. Shi, P. Song *et al.*, 2017 CRISPR/Cas9-based genome editing of the filamentous fungi: the state of the art. Applied Microbiology and Biotechnology 101**:** 7435-7443.

Sipos, G., and K. Kuchler, 2006 Fungal ATP-binding cassette (ABC) transporters in drug resistance & detoxification. Curr Drug Targets 7**:** 471-481.

Sparber, F., C. De Gregorio, S. Steckholzer, F. M. Ferreira, T. Dolowschiak *et al.*, 2019 The skin commensal yeast *Malassezia* triggers a type 17 response that coordinates anti-fungal immunity and exacerbates skin inflammation. Cell Host & Microbe 25**:** 389-403.e386.

Sparber, F., and S. LeibundGut-Landmann, 2017 Host Responses to Malassezia spp. in the Mammalian Skin. Frontiers in Immunology 8**:** 1614.

Triana, S., A. González, R. A. Ohm, H. A. B. Wösten, H. de Cock *et al.*, 2015 Draft genome sequence of the animal and human pathogen *Malassezia pachydermatis* strain CBS 1879. Genome Announcements 3**:** e01197-01115.

Walter, J., J. Urban, C. Volkwein and T. Sommer, 2001 Sec61p-independent degradation of the tail-anchored ER membrane protein Ubc6p. EMBO J 20**:** 3124-3131.

Wang, Q. M., D. Begerow, M. Groenewald, X. Z. Liu, B. Theelen *et al.*, 2015 Multigene phylogeny and taxonomic revision of yeasts and related fungi in the Ustilaginomycotina. Studies in Mycology 81**:** 55-83.

Wang, Q. M., B. Theelen, M. Groenewald, F. Y. Bai and T. Boekhout, 2014 Moniliellomycetes and Malasseziomycetes, two new classes in Ustilaginomycotina. Persoonia 33**:** 41-47.

Wang, Y., and D. J. Burke, 1997 Cdc55p, the B-type regulatory subunit of protein phosphatase 2A, has multiple functions in mitosis and is required for the kinetochore/spindle checkpoint in *Saccharomyces cerevisiae*. Mol Cell Biol 17**:** 620-626.

Wang, Y., D. Wei, X. Zhu, J. Pan, P. Zhang *et al.*, 2016 A 'suicide' CRISPR-Cas9 system to promote gene deletion and restoration by electroporation in *Cryptococcus neoformans*. Scientific Reports 6**:** 31145.

Watanabe, S., R. Kano, H. Sato, Y. Nakamura and A. Hasegawa, 2001 The effects of *Malassezia* yeasts on cytokine production by human keratinocytes. Journal of Investigative Dermatology 116**:** 769-773.

Wrighton, K. H., 2019 *Malassezia restricta* plays CARDs in the gut. Nature Reviews Microbiology 17:266-267.

Wu, G., H. Zhao, C. Li, M. P. Rajapakse, W. C. Wong *et al.*, 2015 Genus-wide comparative genomics of *Malassezia* delineates its phylogeny, physiology, and niche adaptation on human skin. PLoS Genetics 11**:** e1005614.

Xu, J., C. W. Saunders, P. Hu, R. A. Grant, T. Boekhout *et al.*, 2007 Dandruff-associated *Malassezia* genomes reveal convergent and divergent virulence traits shared

with plant and human fungal pathogens. Proceedings of the National Academy of Sciences 104**:** 18730-18735.

Zheng, X., P. Zheng, K. Zhang, T. C. Cairns, V. Meyer *et al.*, 2018 5S rRNA promoter for guide RNA expression enabled highly efficient CRISPR/Cas9 genome editing in *Aspergillus niger*. ACS Synth Biol.

Zhu, Y., P. G. Engstrom, C. Tellgren-Roth, C. D. Baudo, J. C. Kennell *et al.*, 2017 Proteogenomics produces comprehensive and highly accurate protein-coding gene annotation in a complete genome assembly of *Malassezia sympodialis*. Nucleic Acids Res 45**:** 2629-2643.

Figure legends

Figure 1 Southern blot analysis of *M. furfur* insertional mutants selected in the insertional genetic screen as having a phenotype different than the WT. Genomic DNA was digested with SacII, which does not cut within the *NAT* or *NEO* cassette, and hybridized with the ORF of the *NEO* (left) and *NAT* (right) genes. Each hybridization band corresponds to a single T-DNA insertion. The names of the transformants and of the *M. furfur* WT are indicated.

Figure 2 T-DNA insertion sites in 15 transformants of *M. furfur* as determined by iPCR. For each transformant, the mutated region and its corresponding region in the WT are shown. The region altered by the T-DNA is indicated above the sequence. When 2 regions are shown above the sequence, it indicates that the T-DNA insertion involved different locations of the *M. furfur* genome. The borders of the T-DNA are depicted in bold. Uppercase letters represent nucleotides corresponding to regions with RNAseq coverage (and hence representing either 5′ or 3′ UTRs as indicated or ORFs), while lowercase letters represent intergenic regions with no RNAseq coverage. The red nucleotides in strain 6A10 indicate a TAG stop codon. The symbol '-/-' indicates chromosomal rearrangement, with genomic locations shown in parentheses for the 2 transformants (2H11 and 5F10) having rearrangements involving the same chromosome.

Figure 3 Position of T-DNA insertions in *M. furfur* mutants and their associated phenotypes. Each section shows mutants sensitive to the same stress or condition, such as reduced growth on minimal medium YNB (A), reduced growth at 37°C (B), and sensitivity to UV light (C), FLC (D), or cadmium sulfate (E). The positions of the T-DNA insertions are indicated by red bars, and in the same panel the phenotypes of the mutants are also shown. Exons are represented in blue, introns are in white, and UTRs are in gray. In the qPCR of panel 3B **** indicates $p < 0.0001$ and *** indicates $p < 0.001$ ($p = 0.0008$) for each pairwise comparison.

Figure 4 Development of a CRISPR/Cas9 system in *M. furfur*. (A) Complete T-DNA necessary for *CAS9* expression and gRNA excision in *M. furfur*. The promoter and terminator of the histone *H3* gene of *M. sympodialis* ATCC42132 (p*H3* and t*H3*, respectively) and the *CAS9* gene are shown in green. The gRNA is shown in red, and the gene-specific target region is shown in yellow. Sites for recombination (rec) are shown in blue, and the right and left borders (RB and LB, respectively) of the T-DNA are shown in purple. Restriction sites were added to facilitate further molecular manipulation. The black bar indicates the full-length gRNA that is shown in greater resolution in B. (B) The gRNA includes the 5S rRNA promoter region (p5S rRNA) obtained with primers

JOHE46463 and JOHE46464 through touchdown PCR with *M. sympodialis* ATCC42132 genomic DNA. The gene-specific gRNA was obtained by PCR using a target-specific primer, which overlaps with the p5S rRNA and the gRNA scaffold and includes a 20 nt target sequence in between them (represented in yellow). This was used in combination with JOHE46466, which includes the 6T terminator (and also a region for recombination in pPZP201BK, which is not shown). A SpeI restriction site was added to facilitate further use of the CRISPR/Cas9 system in *Malassezia*. To perform targeted mutagenesis of another gene, we recommend using SpeI digestion of the plasmid in A (pGI40) and cloning the 2 PCR products (p5S rRNA and gene-specific gRNA) through Gibson or HiFi assembly. We used this strategy to generate binary vector pGI48 for CRISPR/Cas9-mediated mutagenesis of the *PDR10* gene.

Figure 5: CRISPR/Cas9-mediated target mutagenesis of *M. furfur CDC55*. (A) Co-transformation of *M. furfur* mediated by 2 *A. tumefaciens* strains, one that delivers a T-DNA including the HDR template (ie *cdc55*Δ*::NAT* deletion construct in red) and another that includes the *CAS9* cassette (in green) and the gene-specific gRNA (dark red). Also depicted are the *vir* plasmids present in *A. tumefaciens* cells that are necessary for T-DNA excision and transfer to the *M. furfur* nucleus where homologous recombination occurs. (B) Magnification of the homologous recombination event that occurs in the *M. furfur* nucleus. The top construct represents the T-DNA of the plasmid pGI41 bearing the *cdc55*Δ*::NAT* HDR template. The middle panel represents the native *M. furfur CDC55* locus, the primers used to amplify the 5′ and 3′ regions for HR, the internal primer for the *CDC55* gene, and the 20-nt target sequence (yellow). The gRNA guides Cas9 to the target site to generate a DBS that is repaired using the deletion allele as template, resulting in the targeted replacement of *CDC55* with a *NAT* dominant marker (lower panel). Primers outside the region in which homologous recombination events occur are used in combination with primers for the *NAT* marker to identify *cdc55*Δ mutants. (C) Diagnostic PCR analyses of *M. furfur* WT and NAT-resistant transformants for the identification of *cdc55*Δ mutants. Each panel used the indicated combination of primers, whose position can be found in panel B. PCR primers for *CAS9* and gRNA are reported in Table S1. (D) Phenotypic analysis of *M. furfur* WT, insertional mutant 1A7, and two

independent *cdc55*Δ mutants on mDixon (control), UV (300 µJ x 100), hydroxyurea (50 mM) and benomyl (50 µM); 1.5 µL of tenfold serial dilution were spotted on the agar plates, incubated at 30°C for 3 to 7 days, and then photographed. (E) Microscopic analysis of cell morphology of WT and a representative *cdc55*Δ mutant after growth on mDixon and mDixon supplemented with hydroxyurea (50 mM); the black bar indicates 5 µm.

Figure 6 Targeted CRISPR/Cas9-mediated gene replacement of the *M. furfur PDR10* gene. (A) The T-DNA including the *pdr10*Δ*::NAT* HDR template is shown in the top panel; The *PDR10* gene, the primers used to amplify the 5′ and 3′ regions for homologous recombination, the internal primer for the *PDR10* gene, and the 20-nt target sequence (yellow) for the DBS are shown in the middle panel. The bottom panel shows the *pdr10*Δ mutant allele and the primers used for PCR. (B) Diagnostic PCR analyses of *M. furfur* WT and 5 FLC sensitive and 1 FLC-resistant transformants for the identification of *pdr10*Δ mutants. Each panel used a combination of primers that are represented in panel A. (C) 1.5 µl of cellular suspension of the WT strain CBS 14141, insertional mutant 7D9, and 2 independent *pdr10*Δ mutants were spotted on mDixon (control), FLC (150 µg/mL), amphotericin B (AmB, 50 µg/mL), 5-fluorocytosine (5-FC, 1 mg/mL), caspofungin (Caspo, 100 µg/mL), cyclosporine A alone or with 10 mM of LiCl (CsA, 100 µg/mL), FK506 (100 µg/mL) alone or with 10 mM of LiCl, benomyl (50 µM), UV (300 µJ x 100), hydroxyurea (50 mM), or dimethyl sulfoxide [DMSO, 800 µL/L (solvent used to resuspend benomyl)]. (D) ACT Artemis synteny comparison of a 15-kb region including the 3 copies of the *PDR10* gene of *M. sympodialis* (*Ms*) and the 2 copies of the *PDR10* gene of *M. furfur* (*Mf*). (E) The predicted proteins of the *S. cerevisiae* (*Sc*) ABC transporters Pdr10, Pdr5, Pdr15, Pdr12, Snq2, Pdr18, Aus1, and Pdr11; *M. sympodialis* (*Ms*) Pdr10_1, Pdr10_2, and Pdr10_3; and *M. furfur* (*Mf*) Pdr10_1 and Pdr10_2 were used to generate a maximum likelihood phylogenetic tree with the LG + G method (100 bootstrap replications).

Fig. S1 Phenotypic characterization of putative *M. furfur* cdc55Δ mutants on mDixon + hydroxyurea (50 mM). The *M. furfur* WT strain and 2 transformants that showed increased resistance (R) to hydroxyurea are indicated.

Strains	Phenotype	Hit gene	Position	Comments
1A7	UV	*CDC55*	ORF	Third exon
1F12	CdSO4	NA	NA	NA
2A8	YNB	*ARG1*	ORF	Exon
2F4	$CdSO_4$	*SEC13-PRP43*	*SEC13*-5' region *PRP43*-5' region	Intergenic
2G9	FLC	NA	NA	Tandem insertion
2H11	FLC, NaCl	*ERG5/PDA1*	*ERG5*-ORF / *PDA1*-5' region	Chromosomal rearrangement
3A1	CdSO4	*JLP2/TCP1*	*JLP2*-ORF / *TCP1*-5' region	Chromosomal rearrangement
4A10	NaNO2, SDS	Uncharacterized Enoyl-CoA hydratase	ORF	2 T-DNA insertions
4B1	CdSO4	*MAE1*	3' UTR	2 T-DNA insertions
5D11	FLC	NA	NA	Tandem insertion
5F1	37˚C	*GPD1/INO80*	*GPD1*-5' region/ *INO80*-5' region	Chromosomal rearrangement
5F10	NaCl	*DUG1/RPC10*	*DUG1*-3'UTR / *RPC10*-5'UTR	Chromosomal rearrangement
6A10	FLC	*SIP5*	ORF	Altered stop codon
6B2	37˚C	Uncharacterized Rho GTPase	ORF	2 T-DNA insertions
6C8	YNB	*TYR1* – uncharacterized gene	ORF	Non-standard T-DNA insertion
7D5	37˚C	NA	NA	NA
7D9	FLC	*PDR10-UCB6*	*PDR10*-5' region *UBC6*-3' region	Intergenic
7F8	FLC	*ADY2*	3' UTR	260 bp after the predicted stop codon
7H6	37˚C	*JEN1*- Uncharacterized protein with RNA-binding domain	*JEN1*-5' region unch.-3' region	Intergenic

Table 1 Insertional mutants for *M. furfur* isolated in the forward genetic screen.

NA: inverse PCR failed to identify T-DNA insertions

Table 2 Plasmids used in the present study.

Name	Background	Relevant features	Purpose	References
pAIM2	pPZP-201BK	p*ACT1-NAT*-t*ACT1*	Random insertional mutagenesis	(IANIRI *et al.* 2016)
pAIM6	pPZP-201BK	p*ACT1-NEO*-t*ACT1*	Random insertional mutagenesis	(IANIRI *et al.* 2016)
pPZP-201BK	NA	KAN-R	Binary vector that replicates in *E. coli* and *A. tumefaciens*	(COVERT *et al.* 2001)
pGI3	pPZP-201BK	Sc*URA3* + 2µ; KAN-R	Binary vector that replicates in *E. coli*, *A. tumefaciens* and *S. cerevisiae*	(IANIRI *et al.* 2017)
pGI40	pPZP-201BK	p*H3-CAS9*-t*H3* + p5S rRNA-sgRNA *CDC55*	Cas9 endonuclease and *CDC55* target sgRNA	This study
pGI41	pGI3	*cdc55::NAT*	HDR template to generate *cdc55*Δ	This study
pGI42	pGI3	*pdr10::NAT*	HDR template to generate *pdr10*Δ	This study
pGI48	pGI40	p*H3-CAS9*-t*H3* + p5S rRNA-sgRNA *PDR10*	Cas9 endonuclease and *PDR10_1* target sgRNA	This study

Covert, S. F., P. Kapoor, M.-H. Lee, A. Briley and C. J. Nairn, 2001 Agrobacterium tumefaciens-mediated transformation of Fusarium circinatum. Mycol. Res. 105**:** 259-264.

Ianiri, G., A. F. Averette, J. M. Kingsbury, J. Heitman and A. Idnurm, 2016 Gene function analysis in the ubiquitous human commensal and pathogen Malassezia genus. mBio 7**:** e01853-01816.

Ianiri, G., K. J. Boyce and A. Idnurm, 2017 Isolation of conditional mutations in genes essential for viability of Cryptococcus neoformans. Curr Genet 63**:** 519-530.

Reference

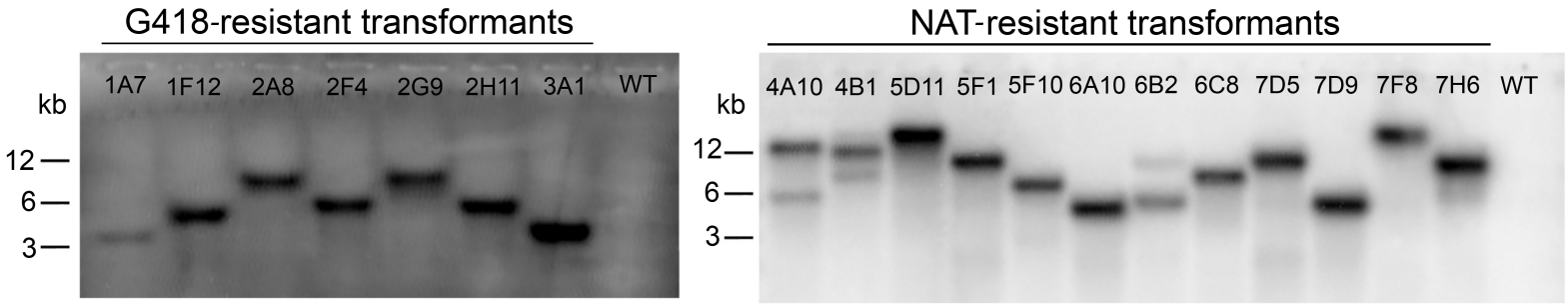

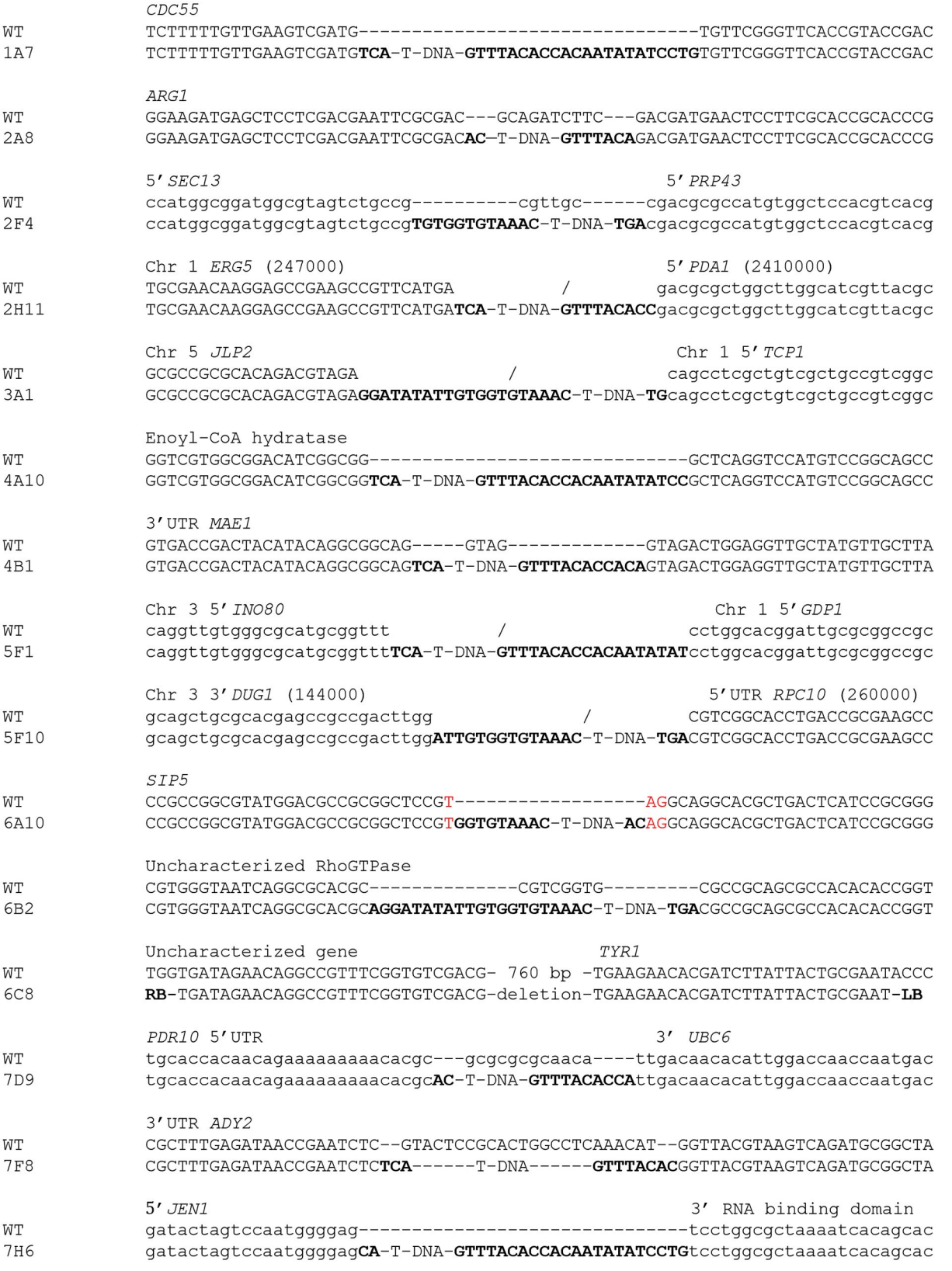
CDC55
WT TCTTTTTGTTGAAGTCGATG----------TGTTCGGGTTCACCGTACCGAC
1A7 TCTTTTTGTTGAAGTCGATGTCA-T-DNA-GTTTACACCACAATATATCCTGTGTTCGGGTTCACCGTACCGAC
ARG1
WT GGAAGATGAGCTCCTCGACGAATTCGCGAC---GCAGATCTTC---GACGATGAACTCCTTCGCACCGCACCCG
2A8 GGAAGATGAGCTCCTCGACGAATTCGCGACAC-T-DNA-GTTTACAGACGATGAACTCCTTCGCACCGCACCCG
5′SEC13 5′PRP43
WT ccatggcggatggcgtagtctgccg----------cgttgc------cgacgcgccatgtggctccacgtcacg
2F4 ccatggcggatggcgtagtctgccgTGTGGTGTAAAC-T-DNA-TGAcgacgcgccatgtggctccacgtcacg
Chr 1 ERG5 (247000) 5′PDA1 (2410000)
WT TGCGAACAAGGAGCCGAAGCCGTTCATGA / gacgcgctggcttggcatcgttacgc
2H11 TGCGAACAAGGAGCCGAAGCCGTTCATGATCA-T-DNA-GTTTACACCgacgcgctggcttggcatcgttacgc
Chr 5 JLP2 Chr 1 5′TCP1
WT GCGCCGCGCACAGACGTAGA / cagcctcgctgtcgctgccgtcggc
3A1 GCGCCGCGCACAGACGTAGAGGATATATTGTGGTGTAAAC-T-DNA-TGcagcctcgctgtcgctgccgtcggc
Enoyl-CoA hydratase
WT GGTCGTGGCGGACATCGGCGG----------GCTCAGGTCCATGTCCGGCAGCC
4A10 GGTCGTGGCGGACATCGGCGGTCA-T-DNA-GTTTACACCACAATATATCCGCTCAGGTCCATGTCCGGCAGCC
3′UTR MAE1
WT GTGACCGACTACATACAGGCGGCAG-----GTAG----------GTAGACTGGAGGTTGCTATGTTGCTTA
4B1 GTGACCGACTACATACAGGCGGCAGTCA-T-DNA-GTTTACACCACAGTAGACTGGAGGTTGCTATGTTGCTTA
Chr 3 5′INO80 Chr 1 5′GDP1
WT caggttgtgggcgcatgcggttt / cctggcacggattgcgcggccgc
5F1 caggttgtgggcgcatgcggtttTCA-T-DNA-GTTTACACCACAATATATcctggcacggattgcgcggccgc
Chr 3 3′DUG1 (144000) 5′UTR RPC10 (260000)
WT gcagctgcgcacgagccgccgacttgg / CGTCGGCACCTGACCGCGAAGCC
5F10 gcagctgcgcacgagccgccgacttggATTGTGGTGTAAAC-T-DNA-TGACGTCGGCACCTGACCGCGAAGCC
SIP5
WT CCGCCGGCGTATGGACGCCGCGGCTCCGT----------AGGCAGGCACGCTGACTCATCCGCGGG
6A10 CCGCCGGCGTATGGACGCCGCGGCTCCGTGGTGTAAAC-T-DNA-ACAGGCAGGCACGCTGACTCATCCGCGGG
Uncharacterized RhoGTPase
WT CGTGGGTAATCAGGCGCACGC----------CGTCGGTG---------CGCCGCAGCGCCACACACCGGT
6B2 CGTGGGTAATCAGGCGCACGCAGGATATATTGTGGTGTAAAC-T-DNA-TGACGCCGCAGCGCCACACACCGGT
Uncharacterized gene TYR1
WT TGGTGATAGAACAGGCCGTTTCGGTGTCGACG- 760 bp -TGAAGAACACGATCTTATTACTGCGAATACCC
6C8 RB-TGATAGAACAGGCCGTTTCGGTGTCGACG-deletion-TGAAGAACACGATCTTATTACTGCGAAT-LB
PDR10 5′UTR 3′ UBC6
WT tgcaccacaacagaaaaaaaaacacgc---gcgcgcgcaaca----ttgacaacacattggaccaaccaatgac
7D9 tgcaccacaacagaaaaaaaaacacgcAC-T-DNA-GTTTACACCAttgacaacacattggaccaaccaatgac
3′UTR ADY2
WT CGCTTTGAGATAACCGAATCTC--GTACTCCGCACTGGCCTCAAACAT--GGTTACGTAAGTCAGATGCGGCTA
7F8 CGCTTTGAGATAACCGAATCTCTCA------T-DNA------GTTTACACGGTTACGTAAGTCAGATGCGGCTA
5′JEN1 3′ RNA binding domain
WT gatactagtccaatggggag----------tcctggcgctaaaatcacagcac
7H6 gatactagtccaatggggagCA-T-DNA-GTTTACACCACAATATATCCTGtcctggcgctaaaatcacagcac

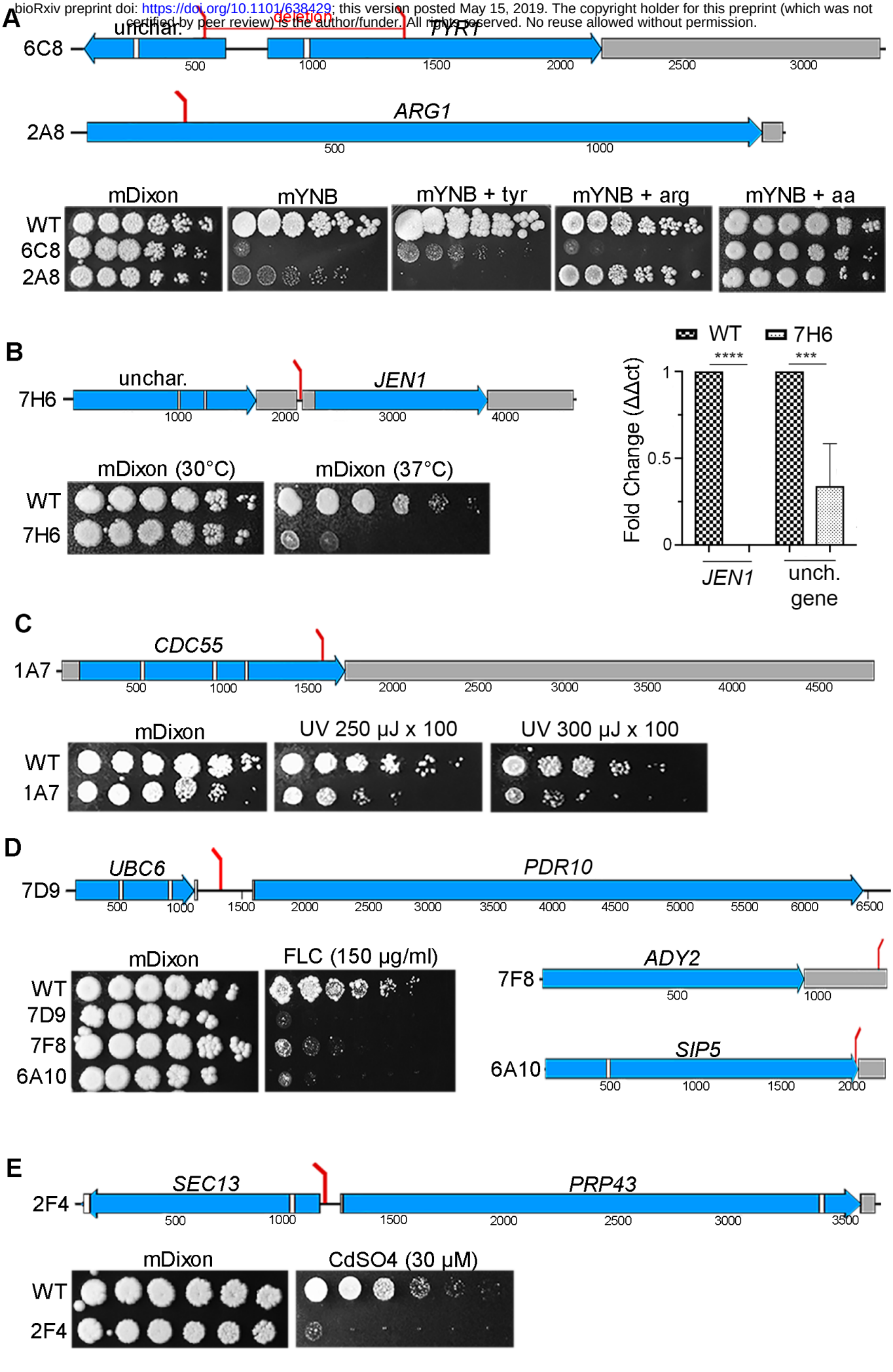

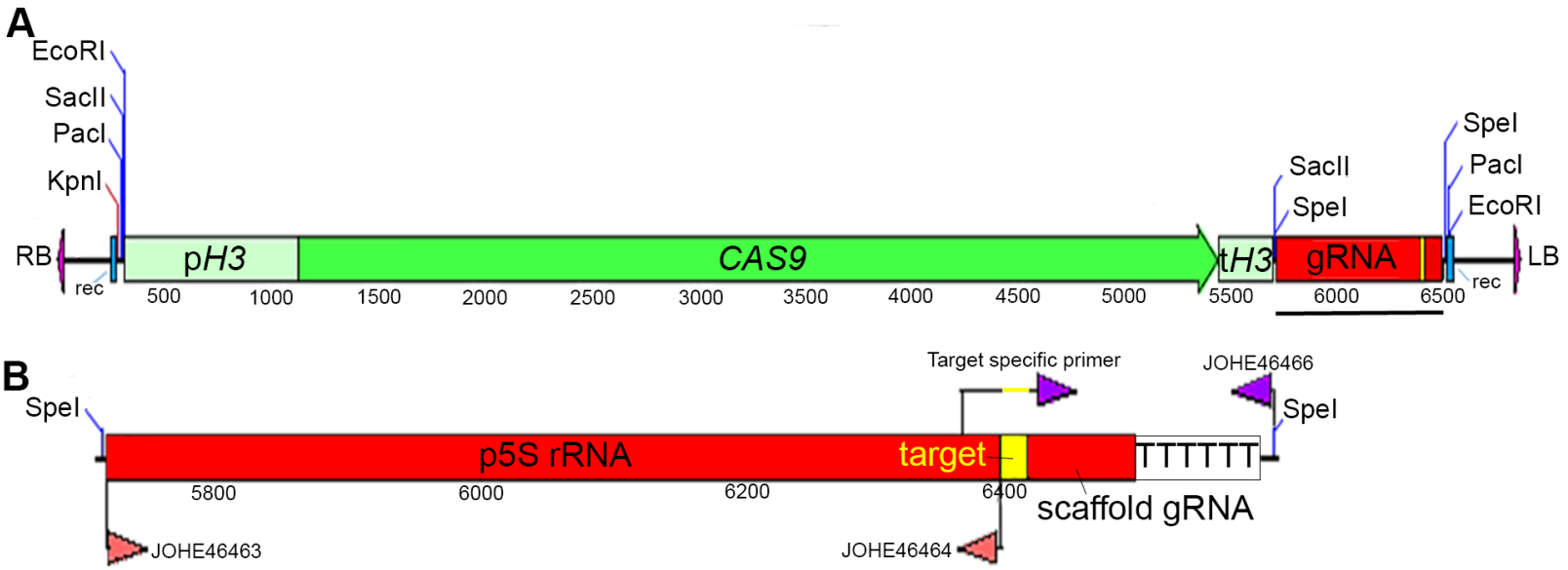

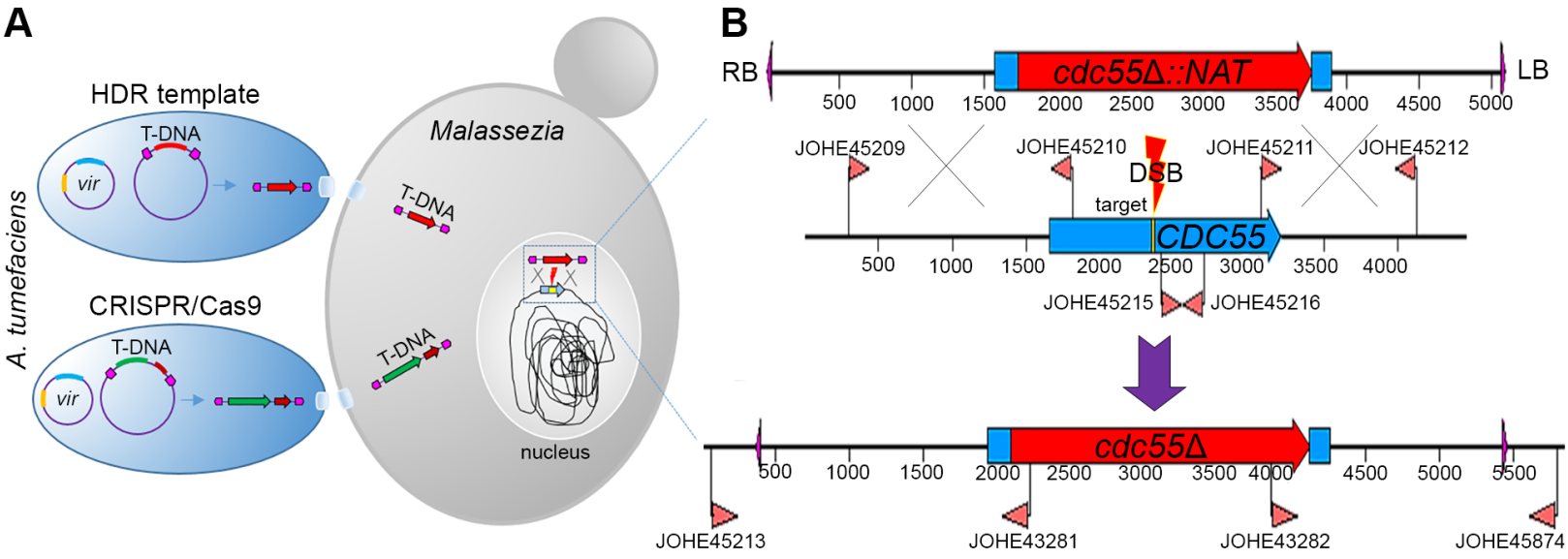

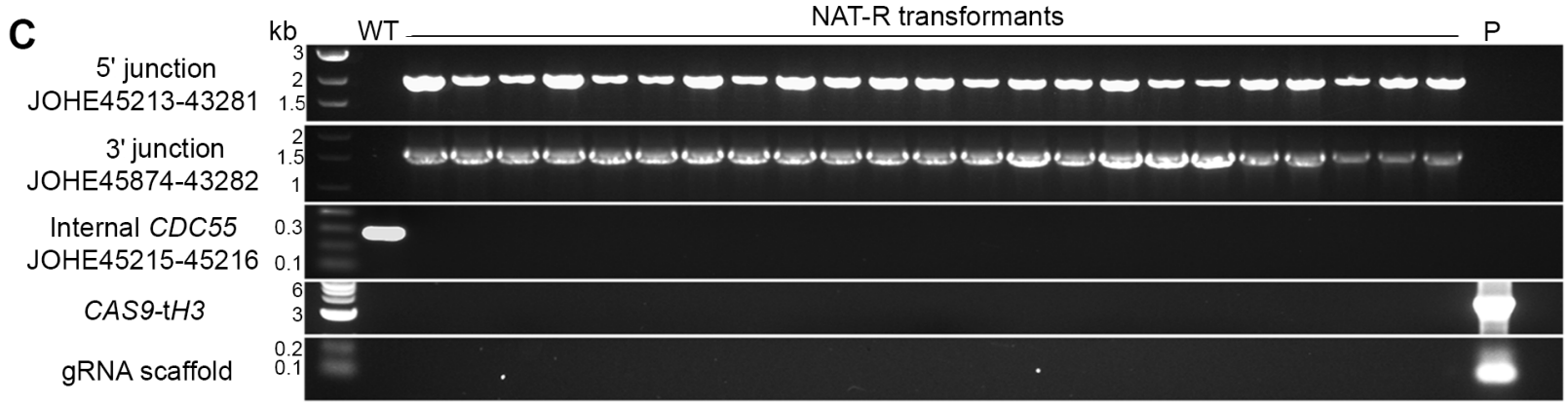

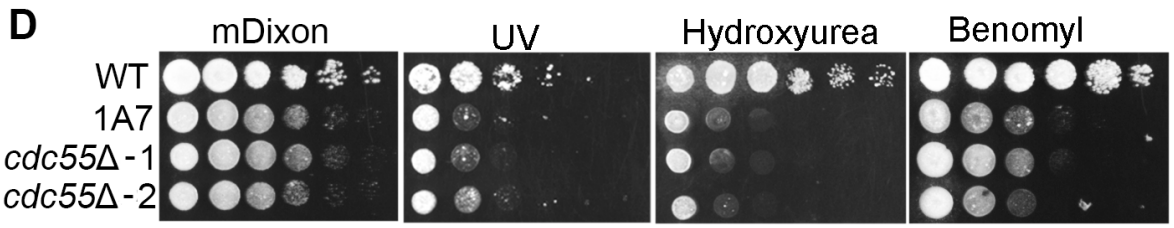

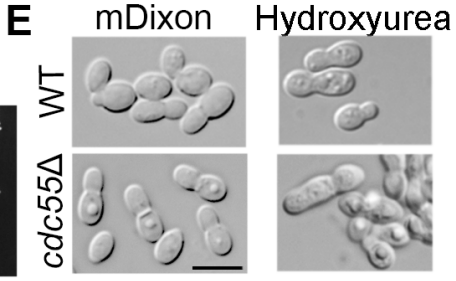

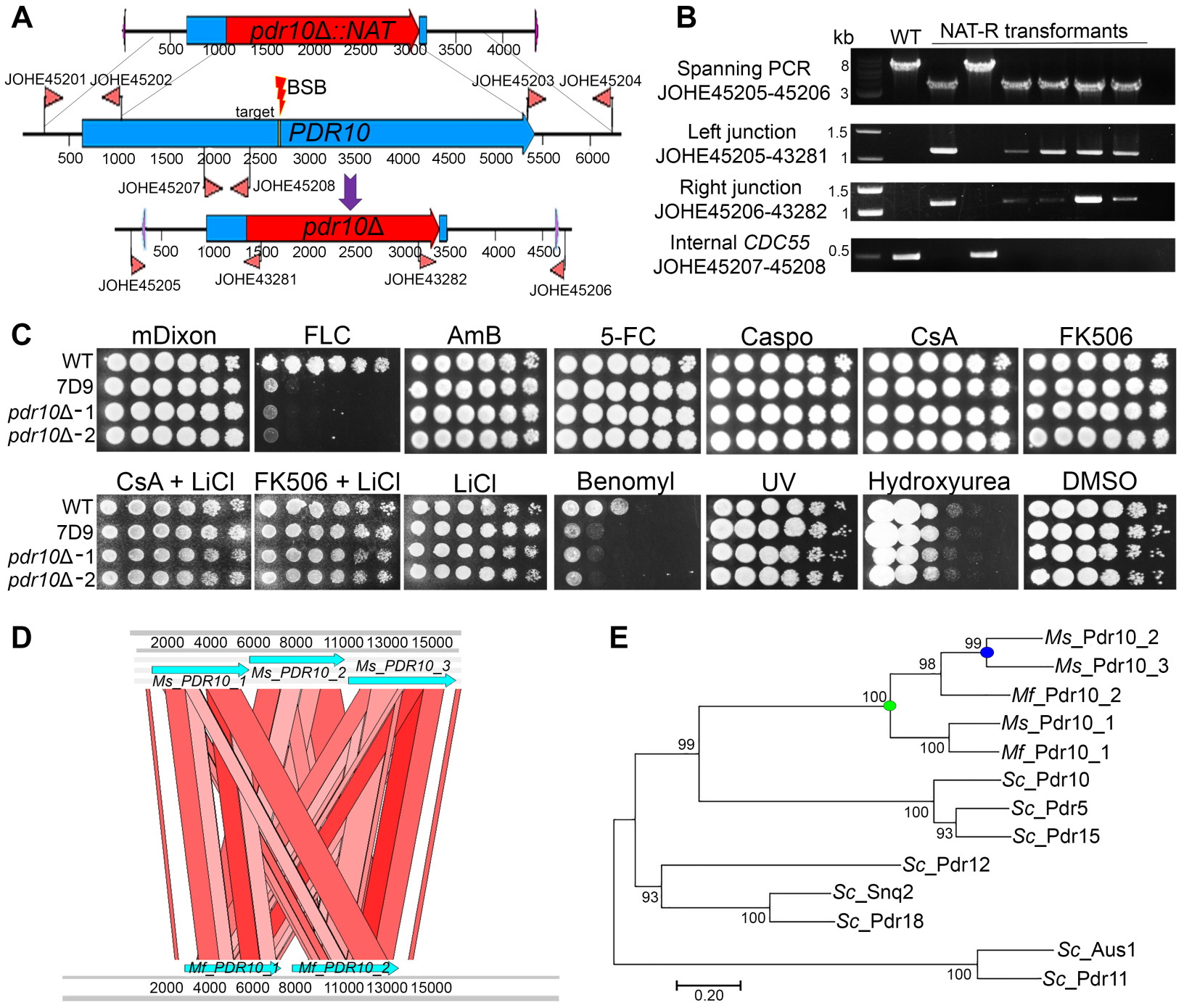

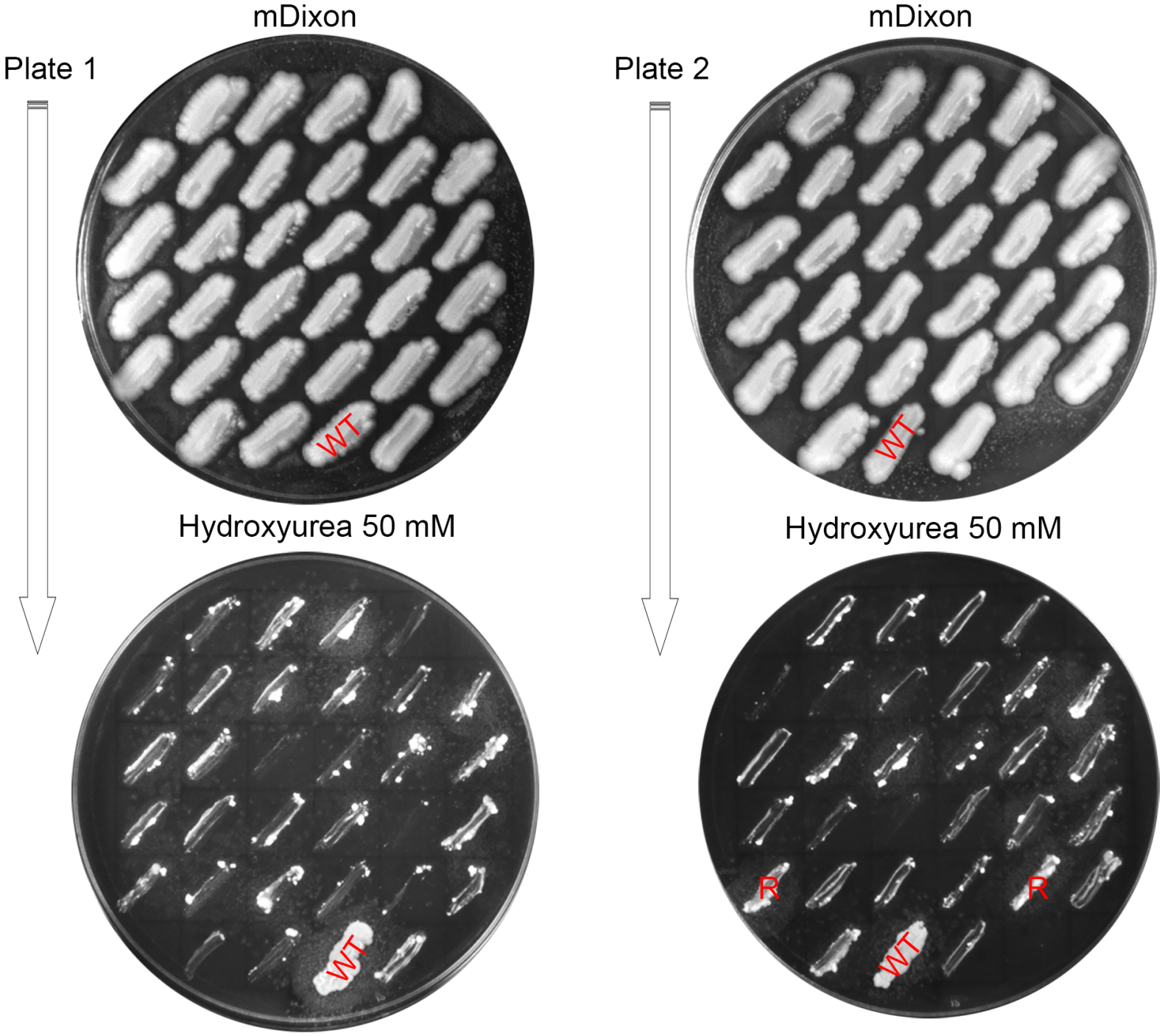

PRIMERS	SEQUENCE 5' - 3'	PURPOSE
M13 F	GTAAAACGACGGCCAGT	NAT and NI
M13 r	CAGGAAACAGCTATGAC	NAT and NI
JOHE43277	TCCACGGTGCAGATCCTC	Malassezia
JOHE43278	CGTCCTCTCCTATGTCTG	Malassezia
ai76	AACAGTTGCGCAGCCTGAATG	inverse PCF
ai77	AGAGGCGGTTTGCGTATTGG	inverse PCF
JOHE43279	CGTATCCAAGCTCAAGCTC	Forward-ch
JOHE43280	GTTGGCCGATTCATTAATGC	Reverse-ch
JOHE43281	GTCGGAGAAGCAGTCAATGC	Reverse-ch
JOHE43282	CACCAGGGTTTCCAGTCTC	Forward-ch
JOHE45201	GCGCGCCTAGGCCTCTGCAGGTCGACTCTggaccagcggaatttctcc	PDR10 5'F
JOHE45202	GAGGATCTGCACCGTGGAgaccaagaagggcaagaagg	PDR10 5'R
JOHE45203	CAGACATAGGAGAGGACGccttcattccacgtctgctt	PDR10 3'F
JOHE45204	TGATTACGAATTCTTAATTAAGATATCGAGaagtcggtcattggttggtc	PDR10 3'R
JOHE45205	cgctggccataaatatcat	PDR10 exte
JOHE45206	taggtcgctagatcggcagt	PDR10 exte
JOHE45207	acacggaaccgataatcagc	PDR10 inte
JOHE45208	aggtggtggtcctgaacaag	PDR10 inte
JOHE45209	GCGCGCCTAGGCCTCTGCAGGTCGACTCTTTCCCCATTCCATCTTTCAG	CDC55 5'F
JOHE45210	GAGGATCTGCACCGTGGATCACCCGTAGCGAGGTAATC	CDC55 5'R
JOHE45211	CAGACATAGGAGAGGACGGAACCCGAACAACATCGACT	CDC55 3'F
JOHE45212	TGATTACGAATTCTTAATTAAGATATCGAGTTGTGCAAGTGATCCAGGAG	CDC55 3'R
JOHE45213	TCCGCAAAATCCTCAATTTC	CDC55 exte
JOHE45874	GCGATGAAGAGGTCGAAGAC	CDC55 exte
JOHE45215	ACCTGGGGATCAGTGACAAG	CDC55 inte
JOHE45216	CTCGGAGAAGAACGACTTGG	CDC55 inte
JOHE46457	GCGCGCCTAGGCCTCTGCAGGTCGACTCT*GGTACCGAGCTCGAT*	pGI3 recom
JOHE46458	gctgtatttttttgtccatTACTCGTAGTAAGAAGCAAC	pH3_R-Cas
JOHE46459	atggacaaaaaatacagc	Cas9 F
JOHE46460	ttaggcgtagtctgggacgtc	Cas9 R
JOHE46461	gacgtcccagactacgcctaaTGGAATCCAAGTGATGTGT	Cas9-f tH3
JOHE46462	GGTGGTTCGACTGTGTCGAACTAGTTTTCCGCGGAAGTCGTCGGGGCTGA	R-tH3-SacII
JOHE46463	CCGCGGAAAACTAGTTCGACACAGTCGAACCACC	F- SacII-Spe
JOHE46464	GAACTGCAGCATCCAGGAT	R-5srRNA
JOHE46465	GTTTTAGAGCTAGAAATAGCAAGTT	Common F
JOHE46466	TGATTACGAATTCTTAATTAAGATATCGAGACTAGTCCGCTCGAGTAAAAC	Common R
JOHE46467	ATCCTGGATGCTGCAGTTCGGTGAAGGTCAGGAGCATCGGTTTTAGA	Furfur_PDR
JOHE46468	ATCCTGGATGCTGCAGTTCGTTGTCGGTGAACTCGGATGGTTTTAGA	Furfur_CDC
JOHE44509/GI	CTTACGTCTAACCAGTCGTC	qPCR_JEN1
JOHE44510	CGAACGAGTTTGGCAGAATC	qPCR_JEN1
JOHE44511	CCCTCATGTCCTCAACACG	qPCR_unch
JOHE44512	GGTTCTTGGTAGATTCTGAT	qPCR_unch
JOHE44515	GCCAGCTGAACTCGGACCTC	qPCR_TUB2
JOHE44516	GCGAGCCCTTGGCAGTCAG	qPCR_TUB2

EO cassette amplification
EO cassette amplification
NAT - F
NAT - R
R
R
ıeck correct recombination with pGI3
eck correct recombination with pGI3
eck correct recombination when using Malassezia NAT gene; screening candidate KO
ıeck correct recombination when using Malassezia NAT gene; screening candidate KO

ernal screen F
ernal screen R
rnal screen F
rnal screen R

ernal screen F
ernal screen R
rnal screen F
rnal screen R
ıb + MCS pH3_F
9

-SpeI-5srRNA
eI-5srRNA

gRNA
gRNA + pGI3 recombination
R12
C55
-F
-R
ıaracterize gene
ıaracterize gene
2-F
2-R